Article

A Multifunctional Supramolecular Hydrogel for Prevention of Epidural Adhesion after Laminectomy

Yan Wang, Lanlan Li, Yongchang Ma, Yong Tang, Yang Zhao, Zimeng Li, Wendan Pu, Bo Huang, Xuan Wen, Xiaojuan Cao, Jiafei Chen, Wei Chen, Yue Zhou, and Jianxiang Zhang

ACS Nano, **Just Accepted Manuscript** • DOI: 10.1021/acsnano.0c01658 • Publication Date (Web): 10 Jun 2020

A Multifunctional Supramolecular Hydrogel for Prevention of Epidural Adhesion after Laminectomy

Yan Wang,[†,¶] Lanlan Li,[+,‡,¶] Yongchang Ma,[+] Yong Tang,[±] Yang Zhao,[+] Zimeng Li,[+] Wendan Pu,[‡] Bo Huang,[†] Xuan Wen,[†] Xiaojuan Cao,[†] Jiafei Chen,[‖] Wei Chen,[‖] Yue Zhou,[*,†] Jianxiang Zhang[*,+,⊥]

[†]Department of Orthopaedic Surgery, Affiliated Xinqiao Hospital, Third Military Medical University (Army Medical University), Chongqing 400037, China

[+]Department of Pharmaceutics, College of Pharmacy, Third Military Medical University (Army Medical University), Chongqing 400038, China

[‡]Department of Chemistry, College of Basic Medicine, Third Military Medical University (Army Medical University), Chongqing 400038, China

[±]Department of Orthopaedic Surgery, The 72 Hospital of Army, Huzhou 313000, China

[‖]Department of Radiology, Southwest Hospital, Third Military Medical University (Army Medical University), Chongqing 400038, China

[⊥]State Key Laboratory of Trauma, Burn and Combined Injury, Institute of Combined Injury, Third Military Medical University (Army Medical University), Chongqing 400038, China

Corresponding authors:

Jianxiang Zhang, PhD, Prof.

E-mail: jxzhang1980@gmail.com, jxzhang@tmmu.edu.cn

Yue Zhou, PhD, Prof.

E-mail: happyzhou@vip.163.com

ABSTRACT: Postoperative epidural adhesion remains a clinically challenging problem in spine surgery. Currently there are no effective and safe anti-fibrotic and anti-adhesion biomaterials that have been specifically developed for this complication in clinical practice. Herein we designed and engineered an advanced anti-adhesion hydrogel with multiple functionalities, including temperature-responsive gelation, self-healing, tissue adhesiveness, anti-oxidation, anti-inflammation, and anti-fibrosis. This multifunctional supramolecular hydrogel can be facilely constructed by integrating three functional modules, *i.e.*, a thermosensitive triblock copolymer poloxamer 407 (PX), a reactive oxygen species-eliminating and anti-inflammatory nanoparticle (TPCD NP), and an adhesion-enhancing compound tannic acid (TA). The optimal formulation (PXNT) was hierarchically screened based on *in vitro* properties and *in vivo* activities. Therapeutically, local treatment with PXNT hydrogel effectively prevented epidural fibrosis and adhesion after laminectomy in both rats and rabbits. Of note, PXNT hydrogel showed more beneficial efficacy than different control thermosensitive hydrogels and a commercially available barrier product Interceed. Mechanistically, PXNT hydrogel significantly attenuated local oxidative stress, inhibited inflammatory responses, and reduced fibrotic tissue formation. Moreover, treatment with PXNT hydrogel did not cause systemic adverse effects and neurological symptoms. Consequently, PXNT hydrogel is a highly promising biomaterial for preventing postlaminectomy epidural adhesion and adhesions after other surgeries.

KEYWORDS: *epidural adhesion, supramolecular hydrogel, self-healing, anti-adhesion, anti-inflammation*

Laminectomy is one of the most common spine surgeries to relieve pressure on the spinal cord or nerve roots. After lumbar laminectomy, however, about 8-40% patients suffered from failed back surgery syndrome (FBSS), such as persistent low back or leg pain resulting from epidural fibrosis due to dura mater compression or peridural tethering.[1, 2] Epidural scar formation also causes neurological symptoms by extensive adhesions around the dura mater and nerve roots, which occur in approximately 24% patients with FBSS.[3] Although improvements in surgical methods and advanced instruments have reduced the incidence of tissue trauma, postoperative epidural fibrosis remains a clinical challenge.[4] Treatment of this complication by secondary surgery is difficult and carries high risks, such as nerve root injuries and dural tears.[5] Consequently, various strategies have been studied to prevent epidural fibrosis and to reduce dural adhesion, such as local or systemic treatment with drugs and using biomaterial-based physical barriers.[6-8] In the biomaterial-based approaches, autologous tissues, natural polymers, and synthetic materials are generally used in the forms of membranes,[9, 10] glues,[11] sponges,[12] and gels.[13-15] In addition, biomaterials are combined with molecular therapeutics to improve anti-fibrotic effects, in which bioactive agents are incorporated in polymeric carriers by either covalent conjugation or physical loading.[10, 16] Despite these advances, however, only a very few biomaterials have entered clinical trials and even fewer been clinically used for prevention of postlaminectomy epidural fibrosis, due to the limited benefits and severe side effects of many currently developed anti-adhesion biomaterials. Different from other postoperative adhesions (such as peritoneal, intrauterine, and tendon adhesions), solid barriers are not appropriate for use around the delicate and vulnerable spinal cord, since a slight compression may result in severe neurological signs. For example, ADCON-L, an anti-adhesion polymer gel, has been banned for clinical use, because of its adverse effects on spinal fusion and muscle healing.[17] As for autologous tissues clinically used to prevent postlaminectomy epidural adhesion,[18] there are also many concerns like dural compression, infection, and necrosis, in addition to their ineffectiveness in some cases.[19, 20] Therefore, novel biomaterials based on rational design are urgently required for effective and safe treatment of epidural fibrosis and fibrous adhesion.

Pathologically, epidural adhesion develops from scar tissue, in which fibroblasts play an important role.[21, 22] Surgery-induced inflammation and hematoma can promote adhesion by affecting fibroblasts.[7] At laminectomy sites, a large number of fibroblasts propagate and produce collagen fibers to repair local vertebral defects after activation by inflammatory cytokines and growth factors, such as tumor necrosis factor (TNF)-α, interleukin (IL)-1, IL-6, and transforming growth factor (TGF)-β.[23, 24] Meanwhile, these molecular mediators are up-regulated by inflammatory cell infiltration relevant to oxidative stress *via* increasing vascular permeability to improve fibroblast proliferation, extracellular matrix synthesis, and eventual scar formation.[7, 23, 24] In addition, oxidative stress-mediated release of reactive oxygen species (ROS) can induce cell injury, promote generation of inflammatory mediators, and exacerbate chronic inflammation. Moreover, chronic nonspecific inflammation may lead to arachnoiditis that is a potential reason of postlaminectomy neurological deficits.[25] Consequently, combination of anti-fibrosis, anti-inflammation, and antioxidative stress should be a promising strategy to prevent postoperative epidural fibrosis and adhesion.

In recent years, sprayable and injectable hydrogels have attracted much attention for local drug delivery,[26, 27] wound repair,[28] tissue regeneration,[29, 30] hemostasis,[31, 32] adhesion prevention,[15, 33-35] and facilitated surgery,[36] owing to their multiple advantages such as easy to use, capability of covering irregular tissues/lesions, as well as minimal invasion and less disturbance to surrounding tissues.[7, 37-39] Although several hydrogel biomaterials have been preliminarily investigated for adhesion prevention after laminectomy,[13-15] the currently developed anti-adhesion hydrogels, particularly those derived from Poloxamer materials have considerable limitations, such as poor tissue adhesiveness. Moreover, these hydrogels only serve as physical barriers to prevent postlaminectomy epidural adhesion, which generally show limited benefits, since they cannot alleviate the local inflammatory responses and oxidative stress. Based on the benefits of injectable hydrogels and according to the pathogenesis of postlaminectomy epidural adhesion, herein we designed an advanced hydrogel by integrating three functional modules *via* a supramolecular approach, which possesses multiple functionalities, including thermosensitive gelation, self-healing, tissue adhesiveness, anti-oxidation, and anti-inflammatory and anti-fibrotic activities.

RESULTS AND DISCUSSION

Design of a Multifunctional Hydrogel for Prevention of Epidural Adhesion. For facile engineering of the mentioned multifunctional hydrogel, Poloxamer 407 (PX), a triblock copolymer of poly(ethylene oxide) and poly(propylene oxide) (PEO-PPO-PEO) broadly used in drug delivery systems,[40] was employed as a hydrogel-forming material (Figure 1A), and its aqueous solutions show excellent thermosensitive sol-gel transition below 37°C.[41] This responsive gelation enables easy and versatile local treatment (such as by spraying) at room temperature, with rapid molding on the target tissues/lesions at body temperature (Figure 1B). Importantly, *in vivo* safety of PX has been extensively demonstrated, particularly after oral or local administration.[42, 43] To endow the engineered hydrogels with desirable bioactivities, we selected a previously developed biocompatible nanotherapy with effective anti-inflammatory and antioxidative stress activities in different animal models of acute and chronic inflammation.[44, 45] To afford bioadhesive capacity, tannic acid (TA), a naturally present compound in many plant species, was introduced in PX hydrogels. As a frequently used feed additive with good safety,[46] a few studies revealed bioadhesive capability of TA in the gastrointestinal and cardiac tissues.[47-49] Also, TA-treated substrates or tissues showed enhanced adhesion to different materials.[50-52] This delicately designed hydrogel owns multiple functions, including thermosensitive *in situ* gelation, self-healing, bioadhesion, anti-inflammation, and anti-oxidation, thereby serving as an effective and easy-handling anti-fibrotic biomaterial to prevent post-laminectomy epidural adhesion (Figure 1C).

Formulation Screening for Engineering a Bioadhesive, Anti-Inflammatory, and Thermosensitive Hydrogel. According to previous findings, hydrogels are formed only when PX concentrations are higher than 12 wt%.[41] While higher concentrations of PX lead to hydrogels with higher strength, the sol-gel transition temperature may also decrease, which is undesirable for local injection in practice. Consequently, PX solutions varying from 16, 18, to 20 wt% were first examined. At these concentrations, rapid gelation was observed at 37°C. Then anti-inflammatory and antioxidative stress nanoparticles were prepared using a broad-spectrum ROS-eliminating material (TPCD) derived from β-cyclodextrin, giving rise to spherical nanoparticles (TPCD

NP) with well-defined shape and relative narrow size distribution (Figure 2A-C). Subsequently, the effects of TPCD NP incorporation on biological functions were examined after local administration in rats subjected to lumbar laminectomy. Compared with the saline-treated model group, TPCD NP at 1 or 5 mg/mL significantly attenuated oxidative stress and inflammation, as implicated by notably decreased levels of peroxide hydrogen (H_2O_2) and IL-6 in fluid wound lavage, independent of PX concentrations (Figure 2D-E). TPCD NP at 0.2 mg/mL, however, showed no significant effects. Furthermore, significant reduction in TGF-β1 was only found for the formulation with 18 wt% PX and 1 mg/mL TPCD NP (*i.e.*, PX18-NP1) (Figure 2F). Of note, abnormally elevated expressions of IL-6 and TGF-β1 are responsible for surgery-induced epidural fibrosis.[53] Nevertheless, gelation occurred even at room temperature (20-25°C) for PX solutions containing 5 mg/mL TPCD NP, regardless of PX concentrations examined (Figure S1), which is undesirable for injection due to high viscosity post gelation.

Based on the above results, formulations containing 1 mg/mL TPCD NP were used for further screening experiments. In this case, TA was introduced to afford bioadhesiveness. To this end, we established an *in vitro* test platform (Figure 2G), in which a tilted plane was covered with bovine spinal dura mater. After hydrogels were dropped onto the plane, the sliding distance was measured to evaluate their relative bioadhesion. For PX18-NP1 hydrogels, dura adhesion considerably increased when the TA content varied from 0, 0.5, 1, to 2 wt% (Figure 2H), which was independent of PX concentrations (Figure 2I). Further increase in TA (such as 3 wt% TA), however, led to formulations that cannot form hydrogel at 37°C (Figure S2). Also, bioadhesive capacity of hydrogels was directly measured using rat muscles (Figure 2J). We observed notably increased adhesive force between two muscle tissues bound together with PX18-NP1 hydrogels, as indicated by the enhanced lap shear stress, when TA changed from 0.5 to 2 wt% (Figure 2K). Notably, focal adhesion-stress of PX18-NP1-TA2 hydrogel (with the formulation of 18 wt% PX, 1 mg/mL TPCD NP, and 2 wt% TA) was almost 4 times higher than that of hydrogel without TA (PX18-NP1-TA0). By contrast, in the presence of urea, a compound that can disrupt hydrogen bonds among different polar groups,[54] bioadhesiveness of PX18-NP1-TA2 hydrogel was significantly reduced (Figure S3). This suggested that hydrogen-bonding between TA and

the components of dura matter or muscle is mainly responsible for bioadhesiveness of TA-containing hydrogels, in line with previous findings on other tissues.[49, 50, 55] Collectively, these results demonstrated that multifunctional hydrogels can be successfully developed by optimally combining three functional modules, *i.e.*, temperature-responsive PX, anti-inflammatory and antioxidative TPCD NP, and bioadhesive TA.

Characterization of Multifunctional Hydrogel. Detailed characterization was then conducted for the finally screened hydrogel derived from 18 wt% PX, 1 mg/mL TPCD NP, and 2 wt% TA, which is abbreviated as PXNT. While PXNT solution is a free-flowing transparent liquid at room temperature, clear sol-gel transition and hydrogel formation were observed at 37°C (Figure 3A). Confocal microscopy observation showed homogenous distribution of Cy5-labeled TPCD NP in FITC-labeled hydrogel (Figure 3B). Scanning electron microscopy (SEM) observation of the fracture surface of lyophilized hydrogel revealed a porous network structure (Figure 3C-D). Embedded nanoparticles were clearly found on the cross-section and sample surface (Figure 3E-F). The presence of different components was also confirmed by FT-IR spectrometry (Figure S4).

Subsequently, rheological studies were performed for PXNT hydrogel. Both storage modulus (G′) and loss modulus (G″) increased with temperature (Figure 3G). Below a specific temperature, G″ was considerably larger than G′, indicating the liquid-state behavior in these cases. By contrast, G′ > G″ was detected upon further increasing temperature, which is a typical characteristic of the solid-like behavior. Thus the sol-gel transition temperature, defined as the intersection point of G′/G″ curves,[56] was determined to be 26.9°C. For aqueous solutions of 18 wt% PX, 18 wt% PX plus 1 mg/mL TPCD NP (PXN), or 18 wt% PX plus 2 wt% TA (PXT), similar temperature-dependent rheological behaviors were observed (Figure S5), with the gelation temperature varied from 23.3, 23.9, to 25.6°C. The relatively high transition temperature of PXNT is more suitable for *in vivo* applications, since its liquid state at room temperature (20-25°C) is a great convenience to cover injured tissues by local injection or spraying. On the other hand, the spinal cord (a very delicate and fragile nerve tissue) is one of the most sensitive parts of the body, and even minor damage may lead to paralysis.[57] Accordingly, the modulus of biomaterials to be used around the spinal cord should be controlled below a critical value.[58] Indeed, stiff materials with high modulus (> 4000 Pa) is likely to cause neurological

symptoms or spinal cord injury.[59] Thus, the relatively low G′ (~3000-3500 Pa at 37°C) of PXNT hydrogel was expected to be suitable.

At 37°C, the sol-gel transition of PXNT occurred within 15 s (Figure 3H). Angular frequent-dependent experiments revealed a nearly linear response for both G′ and G″ within the examined viscoelastic region (Figure 3I). The ratio of G″ to G′ (*i.e.*, tanδ) was calculated to be varied from 0.48 to 0.37 for PXNT as the frequency changed from 0.1 to 100 rad s^{-1} (Figure S6), indicating typical elastic behavior under these conditions. Oscillatory rheology suggested that PXNT hydrogel formed at 37°C was stable when strains varied from 1% to 60%, while it became liquid-like with additional increase in strains (Figure 3J), implying network rupture at high strains. In addition, step-strain experiments were conducted to characterize recovery performance of the dynamic PXNT hydrogel at 37°C, in which a low strain was followed by a high strain (Figure 3K). At a high strain of 200%, fluid-like behavior was observed for PXNT, while it rapidly recovered within 20 s when a low strain (2%) was applied. Notably, this recovery profile was repeatable. Additional steady shear measurement demonstrated shear-thinning behavior of PXNT hydrogel (Figure 3L), as implicated by gradually reduced viscosity when the shear rate extended from 0.1 to 100 s^{-1}. Also, step-shear experiments showed shear-thinning at high shear rates, while rapid recovery appeared at low shear rates (Figure 3M). These results collectively substantiated self-healing capacity of PXNT hydrogel in both stationary and flow-based processes. According to step-strain and step-shear results, the recovery of mechanical properties of PXNT was rapid and repeatable. On the other hand, hydrogel could not be formed by breaking hydrophobic interaction with sodium dodecyl sulfate (Figure S7A), while self-healing capability was considerably impaired by urea (Figure S7B). Therefore, shear-thinning and self-healing of PXNT hydrogel are all attributed to transient rupture of non-covalent crosslinks resulting from hydrophobic and hydrogen-bonding interactions.[33]

Then *in vitro* erosion behaviors of PXNT were tested in 0.9% saline at 37°C. We found gradual erosion of PXNT hydrogel, with complete erosion at day 7 (Figure S8 and Figure 3N). In the absence of TA, PXN hydrogel was completely eroded within 3 days. The erosion result is consistent with the cumulative release profiles of hydrogels (Figure 3O), in which sustained and slowed release of TPCD NP was also observed for

PXNT hydrogel. It is worth noting that nanoparticles released from PXNT hydrogel exhibited size distribution very similar to that of freshly prepared TPCD NP (Figure 3P). Furthermore, after local injection of aqueous solution of PXNT containing Cy7.5-labeled TPCD NP into deep sacrospinalis in rats, relatively long retention of Cy7.5 fluorescence was observed (Figure 3Q), and fluorescence remained at day 7. By contrast, PXN hydrogel maintained for only 3 days *in vivo*. In addition, significantly stronger fluorescence signals were found for PXNT hydrogel at different time points examined, as compared to those of PXN hydrogel (Figure 3R). These results demonstrated that incorporation of TA in PX-based hydrogels can notably reduce their *in vitro* and *in vivo* erosion. Characterization by ^{1}H NMR spectroscopy revealed attenuated proton signals due to methyl groups in PPO, together with peak broadening of signals corresponding to ethylene moieties in the PEO block of PX, in the presence of TA (Figure S9). To a certain degree, proton peaks of phenyl groups in TA were reduced in PXT (*i.e.*, a mixture of PX and TA). Accordingly, on the one hand, TA can promote noncovalent aggregation of the PPO block in PX by its hydrophobic components. On the other hand, TA may interact with PEO or PEG of PX and TPCD NP by hydrogen-bonding *via* its abundant phenolic groups, thereby serving as pseudo-crosslinkers to increase noncovalent interactions among different components of hydrogels and decrease the dissolution of PX molecules in PXNT hydrogel. Consequently, the reduced dissolution of PX should mainly contribute to the relatively low erosion rate of PXNT hydrogel. After lumbar laminectomy, the first phase responsible for the formation of scar tissue is resulted from local inflammatory responses in the first 3-5 days.[8] Consequently, the retention time of 7 days should be appropriate for prevention of epidural fibrosis by the anti-inflammatory strategy based on local delivery of bioactive nanotherapies, in combination with the minimally invasive biomaterial barrier based on dynamic hydrogels.

In a separate study, we also examined the biodistribution of PXNT hydrogel containing Cy5-labeled TPCD NP in the blood and major organs after local injection in deep sacrospinalis of rats. At all detected time points, no Cy5 fluorescence was found in the blood samples (Figure S10). By contrast, significant fluorescence was observed in the liver, spleen, and kidneys at days 1, 3, and 5 after local administration of PXNT hydrogel (Figure S11A), while only slight fluorescence was detected in the heart and lung. Of note, the kidneys showed

higher fluorescence intensities compared to those in the liver and spleen (Figure S11B). Regardless of different organs, fluorescent signals notably decreased at day 7. These preliminary findings revealed a relatively low systemic distribution of locally delivered PXNT hydrogel. In addition, the components of PXNT hydrogel were mainly eliminated by the kidneys. This distribution and excretion performance is beneficial for avoiding possible side effects in other tissues and organs.

***In Vivo* Prevention of Epidural Adhesion after Lumbar Laminectomy in Rats.** Initially, *in vivo* prevention of epidural fibrosis by PXNT was examined in rats. In this case, we used control thermosensitive hydrogels based on a triblock copolymer of poly(lactide-co-glycolide)-*b*-poly(ethylene glycol)-*b*-poly(lactide-co-glycolide) (PLGA-PEG-PLGA, defined as PL) or PL plus TPCD NP (*i.e.*, PLN) that showed transition at 27.9 and 27.7°C, respectively (Figure S12A-B). Likewise, PL and PLN exhibited very similar behaviors in other rheological properties (Figure S12C-H). Notably, PL-based hydrogels exhibited much longer retention time than PX hydrogels after local injection in deep sacrospinalis (Figure S13 and Figure 3Q), although PXNT hydrogel showed considerably higher moduli and bioadhesive capacity than PLN hydrogel (Figure 3G-H, Figure S12A-D, and Figure S14). The local tissue retention of PX- or PL-derived hydrogels is dependent on their erosion behaviors. For physically crosslinked hydrogels, their erosion is not directly related to the magnitude of moduli, whereas hydrogel erosion can indeed considerably reduce their moduli. Nevertheless, the erosion rate of physical hydrogels should be mainly determined by the dissolution rate of gel-forming materials. The dissolution rate of PL and PX used for the hydrogel preparation may be dominated by the mobility of hydrophobic chains, since the hydrophilic PEG/PEO chains of PL and PX will be easily hydrated in aqueous solutions. On the other hand, the chain mobility of polymers is closely associated with their glass transition temperature (T_g). Under similar conditions, polymers with lower T_g exhibit higher chain mobility. As for currently used PL and PX, the corresponding T_g value of the hydrophobic block of PLGA and PPO was estimated to be approximately 30 and -60°C, respectively.[60, 61] As a result, PLGA should have dramatically lower chain mobility than that of PPO, due to the significant difference in T_g. Accordingly, relatively high T_g of the hydrophobic PLGA block in PL should be largely responsible for the long-term tissue retention of PLN

hydrogel. Consistently, *in vitro* tests of PLN hydrogel showed a considerably slower erosion profile, compared to that of PXNT hydrogel (Figure S15 and Figure 3N).

Post laminectomy at the L4 lamina of rats (Figure 4A), different formulations were directly applied on the dura mater. Eight weeks after treatment, gross observation indicated that the dura mater around the laminectomy site was oppressed by severe epidural hardened scars in rats treated with PX, PL, or PLN, and it was difficult to dissect them (Figure 4B). In the PXN group, limited scar tissue was formed, but the epidural adhesion was not severe. By contrast, the PXNT group displayed only soft or weak fibrous tissue around the dura mater, with slight epidural adhesion that could be easily dissected by manual traction without injury to the dura mater. In addition, the dura surface was smooth after the adhesion was removed and the epidural fibrosis (EF) score was only 1.2 ± 0.4 (Figure 4C), the lowest one among all groups.

Furthermore, magnetic resonance (MR) imaging was used to evaluate post-operative epidural fibrosis after intravenous injection of a contrast agent gadolinium-DTPA. For rats treated with PX, PXT, PL, or PLN, their spinal cords were connected with enhanced low signals overlying tissues without clear delineation in either axial or sagittal MR images at week 8 post-operation (Figure 4D). Unexpectedly, both PL and PLN groups even regenerated more scar tissues around the dural sac than the model group. In the PXN group, an incomplete peridural scar was observed at the laminectomy site. As for the PXNT group, there was only a thin peripheral rim of enhancement detected around the dural sac, suggestive of scar granulation tissue but no direct adhesion on the dura. Consistently, quantitative analysis of T1-weighted axial MR images revealed the lowest EF area in the PXNT group (Figure 4E). Similar results were found for MR imaging-based grading scores (Figure 4F-G).

In addition, histological analyses were conducted. At week 8, the outside dural canal was filled with a number of collagen and fibroblasts in the model group, as illustrated by hematoxylin and eosin (H&E)-stained sections (Figure 5A). Histological assessment scores revealed severe adhesion in untreated rats (Figure S16A), and comparable results were found in animals treated with PX. The PL and PLN groups even exhibited more abundant fibroblasts than other groups. Treatment with PXN and PXT resulted in less fibroblasts in epidural scar tissues (Figure S16B). By contrast, the lowest EF score was observed for PXNT-treated rats, indicating

significantly less epidural adhesion in this group. Masson staining revealed serried distribution of dense collagenous tissues around the dura mater in the model group. For rats treated with PXN, dura was slightly attached with the fibrous tissue, and some fibroblasts and sparse collagen fibers were visualized. In the case of the PXNT group, there was a clear interspace between the dura mater and scars, showing slight epidural fibrosis and adhesion (Figure 5B and Figure S16C). The lowest fibrotic area was detected for PXNT-treated rats. By contrast, both PL and PLN groups displayed considerably higher fibrotic area than the model group.

In a separate study, we compared the anti-adhesion effect of PXNT hydrogel with a commercially available product, *i.e.*, Interceed. According to results based on macroscopic observation, MR imaging, and H&E or Masson staining, PXNT-treated rats showed significantly less fibroblast infiltration and fibrotic tissue formation, as compared to those treated with Interceed (Figure 6). Although the Interceed group displayed a blurry gap between dura and fibrotic tissue in histological sections, the gap in sections corresponding to PXNT-treated animals was definitely more explicit. Consequently, our results implied that Interceed had very limited anti-adhesion capacity in the rat model of postlaminectomy epidural fibrosis and adhesion, whereas it can effectively prevent pelvic sidewall, uterine, peritoneal, and peritendinous fibrotic adhesions.[62-65]

***In Vivo* Prevention of Epidural Adhesion after Lumbar Laminectomy in Rabbits.** Next, we examined *in vivo* efficacy of PXNT hydrogel in a rabbit model. Three weeks postsurgery, re-probing the laminectomy site suggested that the PXNT-treated dura mater was easy to expose because of a lack of scar tissue. A thin unmatured fibrous tissue surrounding the dura mater could be easily removed (Left, Figure 7A). In the model group, however, some compact scars were tightly adhered to the dura, which were difficult to separate. Moreover, a separation procedure led to dural sac tears (Right, Figure 7A). Macroscopic assessment revealed significantly decreased EF scores in the PXNT group, compared to the model group (Figure 7B). In addition, MR images revealed a region of low signals (scar tissues) at the laminectomy site in both T1- and T2-weighted axial images in the model group (Upper panel, Figure 7C), which were notably reduced after PXNT treatment. From sagittal images, the spinal cord in the PXNT group exhibited a regular pattern and a linear homogeneous signal separating the dura from the posterior tissue. In the model group, however, the posterior scar tissue was

adhered to the dura and invaded the margin of the spinal canal. Generally, PXNT treatment afforded desirable therapeutic outcomes (Figure 7D). Taken together, these results demonstrated that local treatment with PXNT hydrogels can effectively prevent epidural fibrosis and dural adhesion after lumbar laminectomy in both rats and rabbits. By contrast, PL-based thermosensitive hydrogels showed no any beneficial effects, and only limited benefits were found for a commercial adhesion barrier Interceed.

Mechanistic Studies. Subsequently, mechanisms responsible for the desirable anti-fibrosis and anti-adhesion effects of PXNT hydrogel were examined in rats. During the first 7 days, overall low levels of neutrophils and myeloperoxidase (MPO) in wound lavage fluid were detected for PXNT and PXN groups, particularly the PXNT group at day 7 (Figure 8A-F). The expression levels of TNF-α, IL-1β, and IL-6 were also significantly reduced after treatment with nanotherapy-containing PX hydrogels (Figure 8G-O). In addition, nanotherapy-containing formulations displayed significantly decreased levels of H_2O_2 (Figure 8P-R), a typical and major component of ROS. Of note, PXNT hydrogel resulted in significantly lower H_2O_2 levels after treatment for long periods of time (Figure 8P,R), compared to the model group. These results substantiated that local treatment with PXNT effectively attenuated surgery-induced inflammatory responses and oxidative stress. Treatment with other control formulations, however, showed no or limited beneficial effects on reducing inflammatory cells/cytokines and oxidative mediators. Additionally aggravated inflammatory reactions were even observed for the PL group. For the undesirable effect of PL-based hydrogels, it may be attributed to prolonged exposure of PL near the surgery sites, which can maintain and exacerbate local inflammation by sustainably stimulating peripheral tissues as a foreign body throughout the entire healing process. Furthermore, the PLGA component in PL can be degraded into lactic acid, glycolic acid, and other acidic byproducts, thereby causing local inflammation.[66] Actually, different anti-inflammatory drugs have been used to reduce PLGA-induced inflammatory responses and foreign body reactions for tissue generation.[67, 68] As for TA-containing PXT hydrogel, despite its antioxidant capability to a certain degree, the anti-inflammatory activity was extremely limited in this postlaminectomy rat model.

We also quantified the expression of TGF-β1 (a cytokine mainly excreted by macrophages), in view of its important role in the pathogenesis of fibrosis in different organs/tissues.[69] At all examined time points, notably low levels of TGF-β1 were detected in the PXNT group (Figure 9A-C). Consistently, immunofluorescence analysis of tissues at laminectomy sites at week 8 post-operation revealed the lowest macrophage count in the PXNT group (Figure 9D). These results demonstrated that PXNT hydrogel can also effectively suppress surgery-mediated fibrosis by preventing TGF-β1 production *via* macrophages. Further, these data confirmed the inhibited inflammatory cell infiltration by PXNT, because macrophages are also typical inflammatory cells. In addition, immunofluorescence analysis showed notably reduced $CD31^+$ areas after 8 weeks of treatment with PXNT (Figure 9E), indicating inhibited neovascularization at laminectomy sites. Previous studies demonstrated that angiogenesis is closely associated with fibrosis in different diseases.[70] Collectively, the above results demonstrated that local treatment with our multifunctional hydrogel effectively prevented epidural adhesion after lumbar laminectomy by attenuating inflammatory and oxidative responses as well as inhibiting fibrosis and neovascularization at injured sites.

Safety Studies. Finally, *in vivo* safety of PXNT was examined. During the first 7 days after operation and treatment with various formulations in rats, all groups showed comparable white blood cell counts at different time points (Figure S17). After 4 weeks, PXNT-treated rats showed no abnormal increase in serum levels of typical biomarkers associated with hepatic and renal functions including alanine aminotransferase (ALT), aspartate aminotransferase (AST), and creatinine (CREA), as compared to the model group (Figure S18A-C). Also, the PXNT group exhibited no significant increase in inflammatory cytokines in blood serum (Figure S18D-F). Furthermore, examination on H&E-stained histological sections of major organs from rats treated with different hydrogels revealed no distinguishable injuries and pathological changes (Figure S19). These preliminary results indicated that local treatment with PXNT did not cause systemic adverse effects in rats, in consistent with the finding on biodistribution of PXNT after local injection (Figure S10-11).

At week 8 post-operation, various degrees of neurodegeneration were clearly observed in the model group, as characterized by delamination of the myelin sheath (Figure S20). Myelin sheaths in both PL and PLN groups

were delaminated massively. Also, considerable delamination was found in PX and PXT groups. By contrast, the PXNT group showed negligible abnormalities. Notably, significant delamination was also observed after treatment with the commercial product Interceed (Figure S21A). Subsequently, we evaluated the effects of different treatments on locomotor activity by an open field test based on Basso, Beattie, and Bresnahan (BBB) grading scales. Nearly no alteration in motor function was found for rats in the PXNT group (Figure S22A). However, the results of PL and PLN groups were even worse than those in the model group. Interceed-treated rats also exhibited impaired locomoter activity (Figure S21B). Further, electrophysiological tests showed comparable waveforms of motor-evoked potentials (MEPs) before operation (Pre-OP) and post operation plus PXNT treatment (Post-OP) (Figure S22B). After either 4 or 8 weeks of treatment with PXNT, there were no significant differences in both average latency and amplitude (Figure S22C-D). Together, these results substantiated that local applications of PXNT hydrogel did not cause adverse effects on nerve functions.

CONCLUSIONS

In summary, we engineered a multifunctional hydrogel with anti-inflammatory, anti-oxidative, anti-fibrotic, bioadhesive, self-healing, and thermosensitive properties by rational and facile combination of three functional modules. The optimal hydrogel was developed by hierarchical screening based on *in vitro* properties and *in vivo* activities. *In vivo* studies demonstrated that the finally constructed functional PXNT hydrogel can effectively prevent epidural fibrosis and adhesion after lumbar laminectomy in both rats and rabbits. Compared to other biomaterials currently developed for prevention of postlaminectomy epidural adhesion, PXNT hydrogel has the following advantages: 1) Easy deployment/handling by clinically favorable methods to completely cover the laminectomy sites and simultaneously form an effective physical barrier; 2) Appropriate bioadhesiveness to prevent rapid detachment due to natural movement of the spinal cord; 3) Suitable residence time to achieve clinical benefits but avoid severe foreign body reactions owing to long period of exposure; 4) Desirable viscoelasticity and softness enabling spine mobility and avoiding possible spinal cord/nerve compression; 5) Beneficial anti-oxidative stress, anti-inflammatory, and anti-fibrotic activities to prevent epidural fibrosis; 6)

Good biocompatibility and no impairment to the spinal cord. In addition to lumbar laminectomy, PXNT hydrogel is highly promising for prevention of post-operative adhesions in other conditions, such as stapedectomy, pelvic and abdominal surgery, cardiac surgery, hepatectomy, splenectomy, and nephrectomy, in view of its good safety profile.

EXPERIMENTAL SECTION

Materials. 4-Hydroxy-2,2,6,6-tetramethylpiperidin-1-oxyl (Tempol, abbreviated as Tpl), 4-(hydroxymethyl)phenylboronic acid pinacol ester (PBAP), 1,1-carbonyldiimidazole (CDI), 4-dimethylaminopyridine (DMAP), anhydrous dimethylformamide (DMF), anhydrous dichloromethane (DCM), and anhydrous dimethylsulfoxide (DMSO) were purchased from Sigma-Aldrich (U.S.A.). β-Cyclodextrin (β-CD) and lecithin (from soybean) were obtained from Tokyo Chemical Industry Co., Ltd. (Tokyo, Japan). 1,2-Distearoyl-sn-glycero-3-phosphoethanolamine-N-[methoxy(polyethylene glycol)-2000 (DSPE-PEG) was provided by CordenPharma (Switzerland). Tannic acid (TA), poloxamer 407 (PX), fluorescein-5-isothiocyanate (FITC) were purchased from Sigma-Aldrich (U.S.A.). A triblock copolymer of poly(lactide-co-glycolide)-*b*-poly(ethylene glycol)-*b*-poly(lactide-co-glycolide) (*i.e.*, PLGA-PEG-PLGA abbreviated as PL, M_w of the PLGA and PEG blocks was 1500-2000 and 1000-1500, respectively) was purchased from Daigang Biological Engineering Co., Ltd. (Jinan, China). A commercial absorbable antiadhesion barrier Interceed was obtained from Ethicon Johnson & Johnson (U.S.A.). Cy5 NHS ester (Cy5) and Cy7.5 NHS ester (Cy7.5) were obtained from Lumiprobe, LLC. (U.S.A.). MTT Cell Proliferation and Cytotoxicity Assay Kit was purchased from Beyotime Biotechnology (China). L929 cells were obtained from Bioleaf Biotech (China). Anti-rat HIS48 antibody was purchased from Santa Cruz Biotechnology (U.S.A). Anti-rat CD11b antibody was purchased from Biolegend (U.S.A). Anti-rat CD31 antibody and anti-rat CD68 antibody were purchased from Abcam. Gd-DTPA was obtained from Ruixi Biotechnology (China). Rat MPO Elisa kit were purchased from Jianglai Biotechnology (China). Rat interleukin (IL)-1β, IL-6, tumor necrosis factor (TNF)-α, and tumor growth factor

(TGF)-β1 were purchased from Boster Biological Technology (China). Amplex Red Hydrogen Peroxide kit was obtained from Thermo Fisher (U.S.A). All other reagents are commercially available and used as received.

Synthesis of an Anti-inflammatory and Anti-Oxidative Stress Material TPCD. An anti-inflammatory and anti-oxidative stress material (defined as TPCD) was synthesized according to our previous study.[44] In brief, Tpl (2.04 g, 11.80 mmol) and CDI (3.82 g, 23.61 mmol) were dissolved in anhydrous DCM (20 mL). The obtained mixture was stirred at room temperature for 45 min to obtain CDI-activated Tpl (3.26 g). Then, β-CD (4.70 g, 4.14 mmol) and DMAP (2.26 g, 18.62 mmol) were added to DMSO containing CDI-activated Tpl (3.26 g) and stirred at room temperature for 24 h. Thus obtained product (*i.e.*, TCD) was precipitated from a mixture solution of diethyl ether and methanol. In addition, CDI (3.06 g) and PBAP (2.22 g) were reacted in 30 mL of DCM to give rise to CDI-activated PBAP. Subsequently, TCD (0.84 g), CDI-activated PBAP (3.32 g), and DMAP (2.13 g) were dissolved in 40 mL of anhydrous DMSO. After reaction at room temperature for 2 days, the final product TPCD was collected by precipitation from deionized water, followed by centrifugation and lyophilization.

Preparation and Characterization of TPCD Nanoparticles. TPCD nanoparticles (abbreviated as TPCD NP) were also prepared using our previously established methods.[44] First, lecithin (3 mg) and DSPE-PEG (4.5 mg) were dissolved in 7.5 mL of deionized water at 65°C to obtain an aqueous phase. Then, 25 mg TPCD dissolved in 2.5 mL of methanol was added to the aqueous phase at room temperature. Methanol was removed under reduced pressure to obtain TPCD NP. TPCD NPs labeled with either Cy5 or Cy7.5 were fabricated through similar procedures.

The size and size distribution profiles of TPCD NPs were measured using a Malvern Zetasizer (Nano ZS90, Malvern Instruments, UK) at 25°C. Transmission electron microscopy (TEM) observation of TPCD NP was performed using a TECNAI-10 microscope (Philips, Netherlands). Scanning electron microscopy (SEM) was conducted on a FIB-SEM microscope (Crossbeam 340, Zeiss).

Preparation of Thermosensitive Hydrogels Containing TPCD NP. Appropriate amount of hydrogel-forming materials (PX or PL) was dissolved in Milli-Q water with continuous stirring at 4°C for 3 h. After the

hydrogel-forming material was completely dissolved, aqueous solution of TPCD NP was added to give rise to different thermosensitive hydrogel formulations containing TPCD NP.

Preparation of Multifunctional Hydrogels. First, an appropriate amount of TA was dissolved in Milli-Q water thoroughly with constant stirring at room temperature for 10 min. PX was then added into this TA solution to prepare solutions with varied contents of PX and TA. After aqueous solutions of PX and TA were cooled at 4-5ºC for 24 h, they were mixed with TPCD NP in aqueous solution by magnetic stirring.

Gelation and Rheological Properties of Hydrogels. The test-tube inversion method was employed to determine the gelation performance of different solutions. Briefly, vials containing aqueous solutions of PX, PX plus TPCD NP (PXN), PX plus TPCD NP plus TA (PXNT), or PX plus TA (PXT) were immersed in a water bath at 37°C for 10 min, followed by inverting the vials to confirm the sol-gel transition.

In addition, rheological experiments were performed for different aqueous solutions containing PX and other materials on a rheometer (TA Instruments, U.S.A.) using a parallel plate (plate diameter, 40 mm; gap, 0.05 mm). The storage modulus (G′) and loss modulus (G″') of different combinations were quantified under different conditions. For the temperature-dependent experiments, the heating rate was set at 2.0°C/min. The sol-gel transition temperature was determined as the intersection point of G′ and G″. On the other hand, oscillation strain-dependent changes in G′ and G″ were measured with the shear strain varying from 0.1% to 1000% at 37°C. The oscillation strain corresponding to the sol-gel transition was defined as the intersection point of G′ and G″. Also, time-dependent changes in G′ and G″ values were measured as a function of time at 37°C, with a strain rate of 2%. Frequency-dependent rheological measurements were conducted at 37°C, with a strain rate of 2%. Step-strain measurements were performed at high (200%) and low (2%) strains at 37°C, with an angular frequency of 10 rad s^{-1}. Shear-dependent changes in viscosity and step-shear measurements were carried out at 37°C.

Spectroscopy and Scanning Electron Microscopy. After sample solutions containing different materials were lyophilized, their Fourier transform infrared (FT-IR) spectra were recorded on a PerkinElmer FT-IR spectrometer (S100, U.S.A). ^{1}H NMR spectra of PX, TA, and PX/TA mixture (*i.e.*, PXT) in D_2O were acquired

on a spectrometer operating at 600 MHz (DD2, Agilent). For observation by scanning electron microscopy (SEM), different hydrogel samples were first lyophilized, and then they were fractured to show the internal structures. After coating with gold, morphology observation was performed by SEM (Crossbeam 340, Zeiss).

***In Vitro* Erosion of Hydrogels.** For hydrolysis tests, 2 mL of aqueous solutions containing PXN, PXNT, or PLN was introduced into glass vials that were incubated at 37°C for 10 min. Then 3 mL of 0.9% saline that was preheated to 37°C was added. At predetermined time points, the supernatant was removed. The weight of remaining gel was measured, followed by addition of fresh medium to the initial volume. These procedures were repeated until the hydrogels were completely hydrolyzed.

***In Vitro* Release of TPCD Nanoparticles from Thermosensitive Hydrogels.** For direct assessment of TPCD NP release from PXNT hydrogel, Cy5-labeled TPCD NP was first dispersed in PXT solution with a final concentration of 0.5 mg/mL. Then 3 mL of saline was added to hydrogel gelatinized from 2 mL of aqueous solution of PXNT at 37°C. Samples were kept at 37°C at a shaking speed of 100 rpm. The supernatant was replaced every 24 h. The fluorescence intensity of supernatant was measured on a fluorescence spectrometer (F-7000, Hitach, Japan). The excitation and emission wavelengths were set at 646 and 820 nm, respectively. The cumulative release percentage of TPCD NP was calculated and plotted against time. In addition, the size and size distribution profile of released TPCD NP in the supernatant were measured using a Malvern Zetasizer NanoZS instrument at 25°C.

Animals. All the animal care and experimental protocols were performed in accordance with the guidelines for the Care and Use of Laboratory Animals of Third Military Medical University (Army Medical University, Chongqing, China). Sprague Dawley rats (250-300 g) were obtained from the Animal Center of Daping Hospital. Male New Zealand adult rabbits (3-3.5 kg) were obtained from the Animal Center of Xinqiao Hospital. Animals were housed at a constant temperature (26°C) and relative humidity (70%) with a fixed 12-hour light/dark cycle and free access to food and water. All the animals were acclimatized for 10 days before further experiments. Bovine dura mater was obtained from the Animal Center of the Army Medical University.

***In Vivo* Retention of Thermosensitive Hydrogels.** Aqueous solutions containing PXN or PXNT, in which TPCD NP was labeled with Cy7.5, were injected into deep sacrospinalis with a volume of 0.5 mL. At predetermined time points, all animals were subjected to *in vivo* imaging with an IVIS Spectrum *in vivo* imaging system (PerkinElmer, U.S.A.). The fluorescence intensity was analyzed by the Living Imaging software.

Evaluation of Biodistribution of Locally Injected PXNT. Aqeuous solution of PXNT containing Cy5-labeled TPCD NP was injected into deep sacrospinalis in Sprague Dawley rats. At predetermined time points, animals were euthanized. Blood samples as well as representative organs including heart, liver, spleen, lung, and kidney were collected for *ex vivo* imaging using an IVIS Spectrum *in vivo* imaging system (PerkinElmer, U.S.A.). Fluorescence intensities were analyzed by the Living Imaging software.

***Ex Vivo* Bioadhesion Characterization.** For dura adhesion assessment, a platform with a tilt of 45 degrees was covered with bovine spinal dura mater. Then, 0.5 mL of gelatinized hydrogel was dropped from 5 cm height, and the sliding distance was measured to indirectly evaluate bioadhesive capability of hydrogels.

On the other hand, according to the modified standard test method for strength properties of tissue adhesives (ASTM F2255-05), the muscle adhesion property of hydrogels was assessed using a Test Bench material testing machine (TA Instruments, U.S.A.). The hydrogels were based on different formulations containing 1 mg/mL TPCD NP, 18 wt% PX, and different concentrations of TA (varying from 2 wt%, 1 wt%, 0.5 wt%, to 0 wt%). The lean muscle tissues of rats were used as substrates for the experiments. Hydrogels were applied on one surface of the muscle section (binding area: 10×10 mm^2) and the specimen was covered with another tissue immediately. The bound tissue was loaded until complete separation was achieved. The apparent lap shear stress (in Pa) was calculated as the maximum load divided by the binding area.

Surgery. Under general anesthesia through intraperitoneal injection of pentobarbital sodium in rats at 60 mg/kg, the conventional midline approach was made to get the L4 lumbar area exposed after depilation and disinfection of the surgical region. The L4 lamina was removed with a small laminectomy forceps. After carefully exposing the dura mater, complete hemostasis was carried out. The animals were randomly assigned

to receive different treatments (10 animals in each group). In addition, rats without implantation were included as a model group. After hemostasis, different formulations (0.1 mL per sample) were applied directly on the top of the dura mater gently to serve as a roof structure. About 2 minutes later, the wounds of rats were closed in layers by definite closure of muscle, fascia, and skin. After 8 weeks, epidural fibrosis, material safety assessments, and inflammation evaluations were performed after animals were euthanized.

In separate studies in rats, *in vivo* efficacies of PXNT hydrogel and a commercially available barrier Interceed were compared. In this case, either 0.1 mL of PXTN hydrogel or 0.4 × 0.4 cm^2 membrane of Interceed was gently placed on the top of the dura at the laminectomy sites. At week 3 post-operation, the degrees of epidural fibrosis/adhesion and other assessments were performed after animal were euthanized.

To evaluate anti-adhesion effects of PXNT in rabbits, the operation sites were shaved and sterilized after anesthesia by intravenous injection of pentobarbital *via* the ear vein at 30 mg/kg. After exposure of the L5 lumbar area, the L5 lamina was removed with laminectomy forceps. The animals were randomly assigned to two groups, which were separately treated with either 0.5 mL of PXNT hydrogel or the same volume of saline. After 3 weeks, epidural fibrosis and adhesion degrees as well as other assessments were performed after animals were euthanized.

To quantify the neutrophil counts and the levels of myeloperoxidase (MPO), hydrogen peroxide (H_2O_2), tumor necrosis factor (TNF)-α, interleukin (IL)-1β, IL-6, and transforming growth factor (TGF)-β1, a sterile plastic drainage tube was placed in the surgical area and fixed securely. The animals were subjected to restrictions on the movement in the next 7 days to prevent the tube from pulling out. The surgical region and drainage tubes were disinfected daily. At defined time points, 1 mL of PBS was injected into the wound *via* the drainage tube, and the lavage was collected immediately. Besides, blood samples were collected from the caudal vein for the white blood cell count. Of note, animals suffering from dura lesion, post-operative infection, and immediate neurological deficit were excluded from the experiments.

Quantification of White Blood Cells in the Peripheral Blood and Wound Lavage Fluid. At 6 h, 12 h, 1 d, 2 d, 4 d, and 7 d after surgery, peripheral blood samples were collected *via* the tail vein for the white blood

cell count (Sysmex KX-21, Japan). At the same time points, 1 mL of PBS was injected into the drainage tube as mentioned above, and *in vivo* fluid wound lavage was collected immediately. After three times of lavage, 1 mL of lavage fluid was withdrawn and incubated with red blood cell lysis buffer for 5 min to deplete red blood cells. Then, cells were stained with APC-conjugated rat anti-rat CD11b/c and FITC-conjugated rat anti-rat HIS-48 for analysis by flow cytometry.

Inflammatory Indicators in Wound Lavage. At predetermined time points, *in vivo* lavage fluid was collected as described above. Then 500 μL of Triton X-100 (0.3 wt%) was added into 1.5 mL of residual wound lavage fluid and homogenized, followed by centrifugation at 12000*g* for 10 min at 4°C. The levels of TNF-α, IL-1β, IL-6, TGF-β1, MPO, and H_2O_2 in the supernatant were assessed by ELISA.

Magnetic Resonance Imaging. Magnetic resonance (MR) imaging was carried out at week 8 post-surgery for a total of 70 Sprague Dawley rats (10 rats in each group). MR images were acquired using a Bruker 7.0T MR imaging system. Both sagittal T1/T2-weighted and axial T1/T2-weighted imaging sequences were performed. The T1-weighted set of MR imaging was conducted using the following parameters: repetition time, 800 ms; echo time, 6.0 ms; echo spacing, 6.0 ms; thickness, 0.8 mm; matrix size, 256 × 256. The T2-weighted set of MR imaging was performed according to the following parameters: repetition time, 3000 ms; echo time, 40.0 ms; echo spacing, 13.33 ms; thickness, 0.8 mm; matrix size, 256 × 256. To enhance T1 imaging, a bolus of 0.2 mmol/kg Gd-DTPA was manually injected *via* the rat tail vein 3 min before MR imaging. Similar procedures were followed to compare *in vivo* effects of PXNT hydrogel and Interceed after 3 weeks of treatment.

In addition, MR imaging was carried out for rabbits at week 3 post-surgery using a Siemens Trio Tim 3.0T MRI system. A neck coil (size: 14 cm × 17 cm, 2 channels) was adopted for test. Both axial T1/T2-weighted and sagittal T1/T2-weighted imaging sequences were performed. Parameters for T1- or T2-weighted were set as follows: 10.0 ms echo time and 423.0 ms repetition time for T1; 91.0 ms echo time and 3000.0 ms repetition time for T2. Gd-DTPA was intravenously injected to enhance T1 imaging.

Categorization of the epidural scar tissue was done for three cuts at a determined disc level, with two quadrants per level. Epidural fibrosis (EF) grading was analyzed according to the methods established by Ross *et al*.[71] The degree of EF was graded on a scale of 0-4 for each quadrant at each imaging slice encompassing the operative level: 0 = no to trace scar; 1, 2, 3, 4 = more than trace to 25%, 50%, 75%, and 100%, respectively. In addition, the epidural scar area was measured using the Image J software. MR images were observed by 2 independent investigators in a blinded manner.

Evaluation of Gross Adhesion. At week 8 after surgery, the experimental animals were euthanized, and the surgery sites were probed again. From each group, 10 rats were selected for evaluation of the gross adhesion. To prevent bias, investigators were blinded to the animal information. The degree of adhesion was evaluated based on the Rydell standard.[72] Similar evaluations were performed for rats in comparison studies and for rabbits.

Histological Evaluation. After 8 weeks, the vertebral columns were harvested and fixed for 7 days in a buffer solution (pH 7.4) containing 4% paraformaldehyde. Subsequently, decalcification was performed in 10% EDTA (pH 7.4) at 37°C for 4 weeks. Then, the specimens were dehydrated in graded ethanol and embedded in paraffin. Cross-sections with 4-μm thickness were stained by hematoxylin and eosin (H&E) and Masson's Trichrome for observation. Histological morphometric analyses were performed by quantifying EF grading and the area of the epidural scar tissue. To compare *in vivo* anti-fibrotic effects of PXNT hydrogel with a commercial barrier Interceed in rats, histological evaluations were performed at week 3 postsurgery.

EF grading was performed as follows:[73] Grade 0, no epidural fibrosis, no invasion of adhesive tissues into the spinal canal, and no adhesive tissues on the dura mater; Grade 1, some adhesive tissues invading the margin of the spinal canal although not into it, and only minor fibrous bands on the dura mater; Grade 2, invasion of fibrous tissues into the spinal canal with an adherence ratio less than two thirds of the operative defect; Grade 3, invasion of fibrous tissues with an adherence ratio larger than two thirds of the operative defect; Grade 4, invasion of fibrous tissues completely into the dura sac and referred to the non-operative side and/or the nerve

root; and Grade 5, deformation and retraction of the entire thecal sac accompanied with extensive fibrous tissues.

For qualitative analysis of fibroblast infiltration in H&E-stained sections. The degree of fibroblast infiltration was scored using the following scales: Grade 1, <100 fibroblasts in each 400× field; Grade 2, 100-150 fibroblasts in each 400× field; and Grade 3, >150 fibroblasts in each 400× field.[74] To determine the degree of epidural fibrosis, the EF area was defined by Masson's trichrome staining. The more prominent staining, the more density of fibrosis will be. The percentage of stained area in each 100× field of microscopic views was measured using Image J software.

Immunofluorescence Analysis. Immunofluorescence staining was used to detect the expressions of CD31 and CD68 in epidural fibrosis tissues to examine neovascularization and macrophages, respectively. Briefly, replicate sections were deparaffinized and blocked with 1% BSA and 0.3% Triton X-100 for 30 min at room temperature. Then the sections were incubated with antibodies to CD31 and CD68 at 37°C for 30 min. After 24 h, the slices were incubated with the secondary antibody for 50 min. After nuclei were stained with DAPI, the sections were imaged by confocal laser scanning microscopy. For quantification, normalization by the tissue area from each specimen (n = 10) was used to determine the $CD31^+$ (vessels) and $CD68^+$ (macrophages) areas in each field. All histological slides were observed by two independent investigators in a blinded fashion.

***In Vivo* Safety Evaluation in Rats.** After treatment with different formulations as aforementioned, rats in the model and PXNT groups were enrolled. At week 4, animals were euthanized, and blood samples were collected for biochemical analyses (Olympus AU2700, Japan). The levels of TNF-α, IL-1β, and IL-6 in the blood serum were quantified by ELISA assay. In addition, major organs including heart, liver, spleen, lung, and kidney were isolated and histological sections were prepared and stained with H&E.

TEM Observation of Myelin Sheath Morphology. Examination on myelin sheath morphology was performed at week 8 after different treatments. Briefly, the rat spinal cord was fixed in 2% glutaraldehyde in PBS (pH 7.4) at 4°C for 1 day, post-fixed with 1% osmium tetroxide, dehydrated with increasing concentrations

of ethanol, and embedded. Then, the spinal nerves were put on 0.5% formvar-coated meshes. After staining with uranyl acetate and lead citrate, the spinal nerves were examined *via* TEM (TECNAI-10, Netherlands).

The BBB Locomotor Rating Scale. A locomotor rating scale was selected for nerve function assessment, which was based on the previously published Basso, Beattie, and Bresnahan (BBB) grading scales.[75] BBB scores were collected at week 8 after different treatments.

Electrophysiological Tests. Motor evoked potentials (MEPs) were measured to examine the spinal motor conductions on a Nerve Monitoring System (Medtronic NIM-Eclipse E4, U.S.A.). The recording electrode was inserted into the belly of gastrocnemius muscle in the hind limbs, the reference electrode was inserted near the achilles tendon, and the ground electrode was inserted subcutaneously in the sacrococcygeal region. MEPs were recorded following stimulation of motor cortex through the scalp and skull in order to measure the integrity of the motor neuron. The amplitude and latency data were collected pre-operation, 4 weeks post-operation, and 8 weeks post-operation in the PXNT group.

Statistical Analysis. All data are presented as mean ± standard deviation (SD). Statistical analyses were performed by SPSS 26.0 using one-way ANOVA test for experiments with three or more groups, and unpaired *t*-test was used for data with two groups. Statistical significance was considered at $P < 0.05$.

ASSOCIATED CONTENT

Supporting Information

The Supporting Information is available free of charge on the ACS Publications Website.

Digital photos of aqueous solutions containing varied concentrations of PX and TPCD NP at room temperature; digital photos of aqueous solutions containing various concentrations of PX, TPCD NP, and TA at room or body temperature; the effects of urea on bioadhesiveness of TA-containing hydrogels; FT-IR spectra of various materials; temperature-dependent rheological behaviors of various formulations; angular frequency dependent changes in the values of G″/G′; effects of different additives on gelation and self-healing capacity of PXNT; digital photos showing erosion of hydrogels based on different formulations; ^{1}H NMR spectra of different

materials in D_2O; representative *ex vivo* fluorescence images of blood samples at different time points after local injection in deep sacrospinalis of rats; *in vivo* biodistribution of PXNT hydrogel in major organs after injection in deep sacrospinalis; rheological properties of aqueous solutions containing PL with or without TPCD NP; *in vivo* retention of PL-based hydrogels after intramuscular injection; the quantified sliding distance for PXNT and PLN; *in vitro* erosion of PLN hydrogel; semi-quantitative analysis of the EF degrees based on histological sections; changes in white blood cell counts at various time points after different treatments; *in vivo* safety evaluations after treatment with PXNT hydrogel; H&E-stained histopathological sections of major organs resected from rats subjected to different treatments; TEM images of spinal cord morphology at week 8 after treatment with various formulations; effects of different barriers on spinal cord morphology and motor function; and neurological safety evaluations after different treatments.

AUTHOR INFORMATION

Corresponding Authors

*E-mail: jxzhang1980@gmail.com; jxzhang@tmmu.edu.cn.

*E-mail: happyzhou@vip.163.com

Author Contributions

¶Y.W. and L.L. contributed equally.

ACKNOWLEDGMENTS

This study was supported by the National Natural Science Foundation of China (Nos. 81901866 and 81972114) and the Program for Distinguished Young Scholars of TMMU.

REFERENCES

(1) Guyer, R. D.; Patterson, M.; Ohnmeiss, D. D. Failed Back Surgery Syndrome: Diagnostic Evaluation. *J. Am. Acad. Orthop. Surg.* **2006**, *14*, 534-543.

(2) Chan, C. W.; Peng, P. Failed Back Surgery Syndrome. *Pain Med.* **2011**, *12*, 577-606.

(3) Burton, C. V.; Kirkaldy-Willis, W. H.; Yong-Hing, K.; Heithoff, K. B. Causes of Failure of Surgery on the Lumbar Spine. *Clin. Orthop. Relat. Res.* **1981**, 191-199.

(4) Lee, J. Y.; Stenzel, W.; Impekoven, P.; Theisohn, M.; Stutzer, H.; Lohr, M.; Reithmeier, T.; Ernestus, R. I.; Ebel, H.; Klug, N. The Effect of Mitomycin C in Reducing Epidural Fibrosis after Lumbar Laminectomy in Rats. *J. Neurosurg. Spine* **2006**, *5*, 53-60.

(5) Yakovlev, A. E.; Timchenko, A. A.; Parmentier, A. M. Spinal Cord Stimulation and Sacral Nerve Stimulation for Postlaminectomy Syndrome with Significant Low Back Pain. *Neuromodulation* **2014**, *17*, 763-765.

(6) Gurer, B.; Kahveci, R.; Gokce, E. C.; Ozevren, H.; Turkoglu, E.; Gokce, A. Evaluation of Topical Application and Systemic Administration of Rosuvastatin in Preventing Epidural Fibrosis in Rats. *Spine J.* **2015**, *15*, 522-529.

(7) Wu, W.; Cheng, R.; das Neves, J.; Tang, J.; Xiao, J.; Ni, Q.; Liu, X.; Pan, G.; Li, D.; Cui, W.; Sarmento, B. Advances in Biomaterials for Preventing Tissue Adhesion. *J. Control. Release* **2017**, *261*, 318-336.

(8) Wang, H.; Sun, W.; Fu, D.; Shen, Y.; Chen, Y. Y.; Wang, L. L. Update on Biomaterials for Prevention of Epidural Adhesion after Lumbar Laminectomy. *J. Orthop. Translat.* **2018**, *13*, 41-49.

(9) Sobti, S.; Grover, A.; John, B.; Grewal, S.; George, U. Prospective Randomized Comparative Study to Evaluate Epidural Fibrosis and Surgical Outcome in Patients Undergoing Lumbar Laminectomy with Epidural Autologous Free Fat Graft or Gelfoam: A Preliminary Study. *Int. J. Appl. Basic Med. Res.* **2018**, *8*, 71-75.

(10) Liu, S.; Pan, G.; Liu, G.; Neves, J. D.; Song, S.; Chen, S.; Cheng, B.; Sun, Z.; Sarmento, B.; Cui, W.; Fan, C. Electrospun Fibrous Membranes Featuring Sustained Release of Ibuprofen Reduce Adhesion and Improve Neurological Function Following Lumbar Laminectomy. *J. Control. Release* **2017**, *264*, 1-13.

(11) Cekinmez, M.; Sen, O.; Atalay, B.; Erdogan, B.; Bavbek, M.; Caner, H.; Ozen, O.; Altinors, N. Effects of Methyl Prednisolone Acetate, Fibrin Glue and Combination of Methyl Prednisolone Acetate and Fibrin Glue in Prevention of Epidural Fibrosis in a Rat Model. *Neurol. Res.* **2010**, *32*, 700-705.

(12) Albiñana-Cunningham, J. N.; Ripalda-Cemboráin, P.; Labiano, T.; Echeveste, J. I.; Granero-Moltó, F.; Alfonso-Olmos, M. Mechanical Barriers and Transforming Growth Factor Beta Inhibitor on Epidural Fibrosis in a Rabbit Laminectomy Model. *J. Orthop. Surg. Res.* **2018**, *13*, 72.

(13) Rajiv, S.; Drilling, A.; Bassiouni, A.; Harding, M.; James, C.; Robinson, S.; Moratti, S.; Wormald, P. J. Chitosan Dextran Gel as an Anti Adhesion Agent in a Postlaminectomy Spinal Sheep Model. *J. Clin. Neurosci.* **2017**, *40*, 153-156.

(14) Wang, Y.; Liang, M.; Zheng, Z.; Shi, L.; Su, B.; Liu, J.; Kaplan, D. L.; Zhang, B.; Wang, X. Adhesion Prevention after Laminectomy Using Silk-Polyethylene Glycol Hydrogels. *Adv. Healthc. Mater.* **2015**, *4*, 2120-2127.

(15) Shin, S. J.; Lee, J. H.; So, J.; Min, K. Anti-Adhesive Effect of Poloxamer-Based Thermo-Sensitive Sol-Gel in Rabbit Laminectomy Model. *J. Mater. Sci. Mater. Med.* **2016**, *27*, 162.

(16) Lin, C. Y.; Peng, H. H.; Chen, M. H.; Sun, J. S.; Chang, C. J.; Liu, T. Y.; Chen, M. H. Ibuprofen-Conjugated Hyaluronate/Polygalacturonic Acid Hydrogel for the Prevention of Epidural Fibrosis. *J. Biomater. Appl.* **2016**, *30*, 1589-1600.

(17) Kim, S. B.; Lim, Y. J. Delayed Detected Unexpected Complication of ADCON-L(R) Gel in Lumbar Surgery. *J. Korean Neurosurg. Soc.* **2010**, *48*, 268-271.

(18) Kanamori, M.; Kawaguchi, Y.; Ohmori, K.; Kimura, T.; Tsuji, H.; Matsui, H. The Fate of Autogenous Free-Fat Grafts after Posterior Lumbar Surgery: Part 2. Magnetic Resonance Imaging and Histologic Studies in Repeated Surgery Cases. *Spine* **2001**, *26*, 2264-2270.

(19) Imran, Y.; Halim, Y. Acute Cauda Equina Syndrome Secondary to Free Fat Graft Following Spinal Decompression. *Singapore Med. J.* **2005**, *46*, 25-27.

(20) Gorgulu, A.; Simsek, O.; Cobanoglu, S.; Imer, M.; Parsak, T. The Effect of Epidural Free Fat Graft on the Outcome of Lumbar Disc Surgery. *Neurosurg. Rev.* **2004**, *27*, 181-184.
(21) Sun, Y.; Zhao, S.; Li, X.; Yan, L.; Wang, J.; Wang, D.; Chen, H.; Dai, J.; He, J. Local Application of Rapamycin Reduces Epidural Fibrosis after Laminectomy *via* Inhibiting Fibroblast Proliferation and Prompting Apoptosis. *J. Orthop. Surg. Res.* **2016**, *11*, 58.
(22) Jiao, R.; Chen, H.; Wan, Q.; Zhang, X.; Dai, J.; Li, X.; Yan, L.; Sun, Y. Apigenin Inhibits Fibroblast Proliferation and Reduces Epidural Fibrosis by Regulating Wnt3a/β-Catenin Signaling Pathway. *J. Orthop. Surg. Res.* **2019**, *14*, 258.
(23) Sun, Y.; Wang, L.; Sun, S.; Liu, B.; Wu, N.; Cao, X. The Effect of 10-Hydroxycamptothecine in Preventing Fibroblast Proliferation and Epidural Scar Adhesion after Laminectomy in Rats. *Eur. J. Pharmacol.* **2008**, *593*, 44-48.
(24) Braun, K. M.; Diamond, M. P. The Biology of Adhesion Formation in the Peritoneal Cavity. *Semin. Pediatr. Surg.* **2014**, *23*, 336-343.
(25) Cemil, B.; Kurt, G.; Aydın, C.; Akyurek, N.; Erdogan, B.; Ceviker, N. Evaluation of Tenoxicam on Prevention of Arachnoiditis in Rat Laminectomy Model. *Eur. Spine J.* **2011**, *20*, 1255-1258.
(26) Madry, H.; Gao, L.; Rey-Rico, A.; Venkatesan, J. K.; Müller-Brandt, K.; Cai, X.; Goebel, L.; Schmitt, G.; Speicher-Mentges, S.; Zurakowski, D.; Menger, M. D.; Laschke, M. W.; Cucchiarini, M. Thermosensitive Hydrogel Based on PEO–PPO–PEO Poloxamers for a Controlled *In Situ* Release of Recombinant Adeno-Associated Viral Vectors for Effective Gene Therapy of Cartilage Defects. *Adv. Mater.* **2020**, *32*, 1906508.
(27) Liu, J.; Pang, Y.; Zhang, S.; Cleveland, C.; Yin, X.; Booth, L.; Lin, J.; Lucy Lee, Y.-A.; Mazdiyasni, H.; Saxton, S.; Kirtane, A. R.; von Erlach, T.; Rogner, J.; Langer, R.; Traverso, G. Triggerable Tough Hydrogels for Gastric Resident Dosage Forms. *Nat. Commun.* **2017**, *8*, 124.
(28) Dimatteo, R.; Darling, N. J.; Segura, T. *In Situ* Forming Injectable Hydrogels for Drug Delivery and Wound Repair. *Adv. Drug Deliv. Rev.* **2018**, *127*, 167-184.
(29) Shirzaei Sani, E.; Portillo Lara, R.; Aldawood, Z.; Bassir, S. H.; Nguyen, D.; Kantarci, A.; Intini, G.; Annabi, N. An Antimicrobial Dental Light Curable Bioadhesive Hydrogel for Treatment of Peri-Implant Diseases. *Matter* **2019**, *1*, 926-944.
(30) Bai, S.; Zhang, X.; Lv, X.; Zhang, M.; Huang, X.; Shi, Y.; Lu, C.; Song, J.; Yang, H. Bioinspired Mineral–Organic Bone Adhesives for Stable Fracture Fixation and Accelerated Bone Regeneration. *Adv. Funct. Mater.* **2020**, *30*, 1908381.
(31) Liang, Y.; Zhao, X.; Hu, T.; Chen, B.; Yin, Z.; Ma, P. X.; Guo, B. Adhesive Hemostatic Conducting Injectable Composite Hydrogels with Sustained Drug Release and Photothermal Antibacterial Activity to Promote Full-Thickness Skin Regeneration During Wound Healing. *Small* **2019**, *15*, 1900046.
(32) Zhao, X.; Guo, B.; Wu, H.; Liang, Y.; Ma, P. X. Injectable Antibacterial Conductive Nanocomposite Cryogels with Rapid Shape Recovery for Noncompressible Hemorrhage and Wound Healing. *Nat. Commun.* **2018**, *9*, 2784.
(33) Stapleton, L. M.; Steele, A. N.; Wang, H.; Lopez Hernandez, H.; Yu, A. C.; Paulsen, M. J.; Smith, A. A. A.; Roth, G. A.; Thakore, A. D.; Lucian, H. J.; Totherow, K. P.; Baker, S. W.; Tada, Y.; Farry, J. M.; Eskandari, A.; Hironaka, C. E.; Jaatinen, K. J.; Williams, K. M.; Bergamasco, H.; Marschel, C*., et al.* Use of a Supramolecular Polymeric Hydrogel as an Effective Post-Operative Pericardial Adhesion Barrier. *Nat. Biomed. Eng.* **2019**, *3*, 611-620.
(34) Li, L.; Wang, N.; Jin, X.; Deng, R.; Nie, S.; Sun, L.; Wu, Q.; Wei, Y.; Gong, C. Biodegradable and Injectable *In Situ* Cross-Linking Chitosan-Hyaluronic Acid Based Hydrogels for Postoperative Adhesion Prevention. *Biomaterials* **2014**, *35*, 3903-3917.
(35) Zhang, Z.; Ni, J.; Chen, L.; Yu, L.; Xu, J.; Ding, J. Biodegradable and Thermoreversible PCLA-PEG-PCLA Hydrogel as a Barrier for Prevention of Post-Operative Adhesion. *Biomaterials* **2011**, *32*, 4725-4736.
(36) Pang, Y.; Liu, J.; Moussa, Z. L.; Collins, J. E.; McDonnell, S.; Hayward, A. M.; Jajoo, K.; Langer, R.; Traverso, G. Endoscopically Injectable Shear-Thinning Hydrogels Facilitating Polyp Removal. *Adv. Sci.* **2019**, *6*, 1901041.

(37) Zhou, H.; Liang, C. Y.; Wei, Z.; Bai, Y. J.; Bhaduri, S. B.; Webster, T. J.; Bian, L. M.; Yang, L. Injectable Biomaterials for Translational Medicine. *Mater. Today* **2019**, *28*, 81-97.
(38) Chivers, P. R. A.; Smith, D. K. Shaping and Structuring Supramolecular Gels. *Nat. Rev. Mater.* **2019**, *4*, 463-478.
(39) Annabi, N.; Tamayol, A.; Uquillas, J. A.; Akbari, M.; Bertassoni, L. E.; Cha, C.; Camci-Unal, G.; Dokmeci, M. R.; Peppas, N. A.; Khademhosseini, A. Rational Design and Applications of Hydrogels in Regenerative Medicine. *Adv. Mater.* **2014**, *26*, 85-124.
(40) Akash, M. S. H.; Rehman, K. Recent Progress in Biomedical Applications of Pluronic (PF127): Pharmaceutical Perspectives. *J. Control. Release* **2015**, *209*, 120-138.
(41) Fakhari, A.; Corcoran, M.; Schwarz, A. Thermogelling Properties of Purified Poloxamer 407. *Heliyon* **2017**, *3*, e00390.
(42) Singh-Joy, S. D.; McLain, V. C. Safety Assessment of Poloxamers 101, 105, 108, 122, 123, 124, 181, 182, 183, 184, 185, 188, 212, 215, 217, 231, 234, 235, 237, 238, 282, 284, 288, 331, 333, 334, 335, 338, 401, 402, 403, and 407, Poloxamer 105 Benzoate, and Poloxamer 182 Dibenzoate as Used in Cosmetics. *Inter. J. Toxicol.* **2008**, *27*, 93-128.
(43) Strickley, R. G. Solubilizing Excipients in Oral and Injectable Formulations. *Pharm. Res.* **2004**, *21*, 201-230.
(44) Li, L.; Guo, J.; Wang, Y.; Xiong, X.; Tao, H.; Li, J.; Jia, Y.; Hu, H.; Zhang, J. A Broad-Spectrum ROS-Eliminating Material for Prevention of Inflammation and Drug-Induced Organ Toxicity. *Adv. Sci.* **2018**, *5*, 1800781.
(45) Wang, Y.; Li, L.; Zhao, W.; Dou, Y.; An, H.; Tao, H.; Xu, X.; Jia, Y.; Lu, S.; Zhang, J.; Hu, H. Targeted Therapy of Atherosclerosis by a Broad-Spectrum Reactive Oxygen Species Scavenging Nanoparticle with Intrinsic Anti-Inflammatory Activity. *ACS Nano* **2018**, *12*, 8943-8960.
(46) EFSA Panel on Additives and Products or Substances used in Animal Feed (FEEDAP). Scientific Opinion on the Safety and Efficacy of Tannic Acid When Used as Feed Flavouring for All Animal Species. *EFSA J.* **2014**, *12*, 3828.
(47) Shin, M.; Kim, K.; Shim, W.; Yang, J. W.; Lee, H. Tannic Acid as a Degradable Mucoadhesive Compound. *ACS Biomater. Sci. Eng.* **2016**, *2*, 687-696.
(48) Guo, J.; Sun, W.; Kim, J. P.; Lu, X.; Li, Q.; Lin, M.; Mrowczynski, O.; Rizk, E. B.; Cheng, J.; Qian, G.; Yang, J. Development of Tannin-Inspired Antimicrobial Bioadhesives. *Acta Biomater.* **2018**, *72*, 35-44.
(49) Shin, M.; Lee, H.-A.; Lee, M.; Shin, Y.; Song, J.-J.; Kang, S.-W.; Nam, D.-H.; Jeon, E. J.; Cho, M.; Do, M.; Park, S.; Lee, M. S.; Jang, J.-H.; Cho, S.-W.; Kim, K.-S.; Lee, H. Targeting Protein and Peptide Therapeutics to the Heart *via* Tannic Acid Modification. *Nat. Biomed. Eng.* **2018**, *2*, 304-317.
(50) Li, B.; Whalen, J. J.; Humayun, M. S.; Thompson, M. E. Reversible Bioadhesives Using Tannic Acid Primed Thermally-Responsive Polymers. *Adv. Funct. Mater.* **2020**, *30*, 1907478.
(51) Nam, H. G.; Nam, M. G.; Yoo, P. J.; Kim, J.-H. Hydrogen Bonding-Based Strongly Adhesive Coacervate Hydrogels Synthesized Using Poly(N-Vinylpyrrolidone) and Tannic Acid. *Soft Matter* **2019**, *15*, 785-791.
(52) Wang, Z.; Zhao, S.; Song, R.; Zhang, W.; Zhang, S.; Li, J. The Synergy between Natural Polyphenol-Inspired Catechol Moieties and Plant Protein-Derived Bio-Adhesive Enhances the Wet Bonding Strength. *Sci. Rep.* **2017**, *7*, 9664.
(53) Yang, L.; Tang, J.; Chen, H.; Ge, D.; Sui, T.; Que, J.; Cao, X.; Ge, Y. Taurine Reduced Epidural Fibrosis in Rat Models after Laminectomy *via* Downregulating EGR1. *Cell. Physiol. Biochem.* **2016**, *38*, 2261-2271.
(54) Bennion, B. J.; Daggett, V. The Molecular Basis for the Chemical Denaturation of Proteins by Urea. *Proc. Natl. Acad. Sci. U. S. A.* **2003**, *100*, 5142-5147.
(55) Rahim, M. A.; Kristufek, S. L.; Pan, S.; Richardson, J. J.; Caruso, F. Phenolic Building Blocks for the Assembly of Functional Materials. *Angew. Chem. Int. Ed.* **2019**, *58*, 1904-1927.
(56) Onoda, M.; Ueki, T.; Tamate, R.; Shibayama, M.; Yoshida, R. Amoeba-Like Self-Oscillating Polymeric Fluids with Autonomous Sol-Gel Transition. *Nat. Commun.* **2017**, *8*, 15862.
(57) McDonald, J. W.; Sadowsky, C. Spinal-Cord Injury. *Lancet* **2002**, *359*, 417-425.

(58) Assuncao-Silva, R. C.; Gomes, E. D.; Sousa, N.; Silva, N. A.; Salgado, A. J. Hydrogels and Cell Based Therapies in Spinal Cord Injury Regeneration. *Stem Cells Int.* **2015**, *2015*, 948040.
(59) Bakshi, A.; Fisher, O.; Dagci, T.; Himes, B. T.; Fischer, I.; Lowman, A. Mechanically Engineered Hydrogel Scaffolds for Axonal Growth and Angiogenesis after Transplantation in Spinal Cord Injury. *J. Neurosurg. Spine* **2004**, *1*, 322-329.
(60) In Pyo Park, P.; Jonnalagadda, S. Predictors of Glass Transition in the Biodegradable Poly-Lactide and Poly-Lactide-Co-Glycolide Polymers. *J. Appl. Polym. Sci.* **2006**, *100*, 1983-1987.
(61) Faucher, J. A. The Dependence of Glass Transition Temperature on Molecular Weight for Poly(Propylene Oxide) and Poly(Butylene Oxide). *J. Polym. Sci. B Polym. Lett.* **1965**, *3*, 143-145.
(62) Azziz, R. Microsurgery Alone or with INTERCEED Absorbable Adhesion Barrier for Pelvic Sidewall Adhesion Re-Formation. The INTERCEED (TC7) Adhesion Barrier Study Group II. *Surg. Gynecol. Obstet.* **1993**, *177*, 135-139.
(63) Marshburn, P. B.; Meek, J. M.; Gruber, H. E.; Gordon, B. E.; Norton, J. H.; Hurst, B. S. Preoperative Leuprolide Acetate Combined with Interceed* Optimally Reduces Uterine Adhesions and Fibrosis in a Rabbit Model. *Fertil. Steril.* **2004**, *81*, 194-197.
(64) Gago, L. A.; Saed, G.; Elhammady, E.; Diamond, M. P. Effect of Oxidized Regenerated Cellulose (Interceed) on the Expression of Tissue Plasminogen Activator and Plasminogen Activator Inhibitor-1 in Human Peritoneal Fibroblasts and Mesothelial Cells. *Fertil. Steril.* **2006**, *86*, 1223-1227.
(65) Temiz, A.; Ozturk, C.; Bakunov, A.; Kara, K.; Kaleli, T. A New Material for Prevention of Peritendinous Fibrotic Adhesions after Tendon Repair: Oxidised Regenerated Cellulose (Interceed), an Absorbable Adhesion Barrier. *Int. Orthop.* **2008**, *32*, 389-394.
(66) Kim, M. S.; Ahn, H. H.; Shin, Y. N.; Cho, M. H.; Khang, G.; Lee, H. B. An *In Vivo* Study of the Host Tissue Response to Subcutaneous Implantation of PLGA- and/or Porcine Small Intestinal Submucosa-Based Scaffolds. *Biomaterials* **2007**, *28*, 5137-5143.
(67) Thevenot, P. T.; Nair, A. M.; Shen, J.; Lotfi, P.; Ko, C. Y.; Tang, L. The Effect of Incorporation of SDF-1alpha into PLGA Scaffolds on Stem Cell Recruitment and the Inflammatory Response. *Biomaterials* **2010**, *31*, 3997-4008.
(68) Lee, Y.; Kwon, J.; Khang, G.; Lee, D. Reduction of Inflammatory Responses and Enhancement of Extracellular Matrix Formation by Vanillin-Incorporated Poly(Lactic-Co-Glycolic Acid) Scaffolds. *Tissue Eng. Part A* **2012**, *18*, 1967-1978.
(69) Munger, J. S.; Huang, X.; Kawakatsu, H.; Griffiths, M. J. D.; Dalton, S. L.; Wu, J.; Pittet, J.-F.; Kaminski, N.; Garat, C.; Matthay, M. A.; Rifkin, D. B.; Sheppard, D. A Mechanism for Regulating Pulmonary Inflammation and Fibrosis: The Integrin Avβ6 Binds and Activates Latent TGF B1. *Cell* **1999**, *96*, 319-328.
(70) Elpek, G. Ö. Angiogenesis and Liver Fibrosis. *World J. Hepatol.* **2015**, *7*, 377-391.
(71) Ross, J. S.; Obuchowski, N.; Modic, M. T. MR Evaluation of Epidural Fibrosis: Proposed Grading System with Intra- and Inter-Observer Variability. *Neurol. Res.* **1999**, *21*, S23-26.
(72) Sun, Y.; Wang, L. X.; Wang, L.; Sun, S. X.; Cao, X. J.; Wang, P.; Feng, L. A Comparison of the Effectiveness of Mitomycin C and 5-Fluorouracil in the Prevention of Peridural Adhesion after Laminectomy. *J. Neurosurg. Spine* **2007**, *7*, 423-428.
(73) Tseng, Y. Y.; Liao, J. Y.; Chen, W. A.; Kao, Y. C.; Liu, S. J. Biodegradable Poly([D,L]-Lactide-Co-Glycolide) Nanofibers for the Sustainable Delivery of Lidocaine into the Epidural Space after Laminectomy. *Nanomedicine* **2014**, *9*, 77-87.
(74) Coskun, E.; Suzer, T.; Topuz, O.; Zencir, M.; Pakdemirli, E.; Tahta, K. Relationships between Epidural Fibrosis, Pain, Disability, and Psychological Factors after Lumbar Disc Surgery. *Eur. Spine J.* **2000**, *9*, 218-223.
(75) Basso, D. M.; Beattie, M. S.; Bresnahan, J. C. A Sensitive and Reliable Locomotor Rating Scale for Open Field Testing in Rats. *J. Neurotrauma* **1995**, *12*, 1-21.

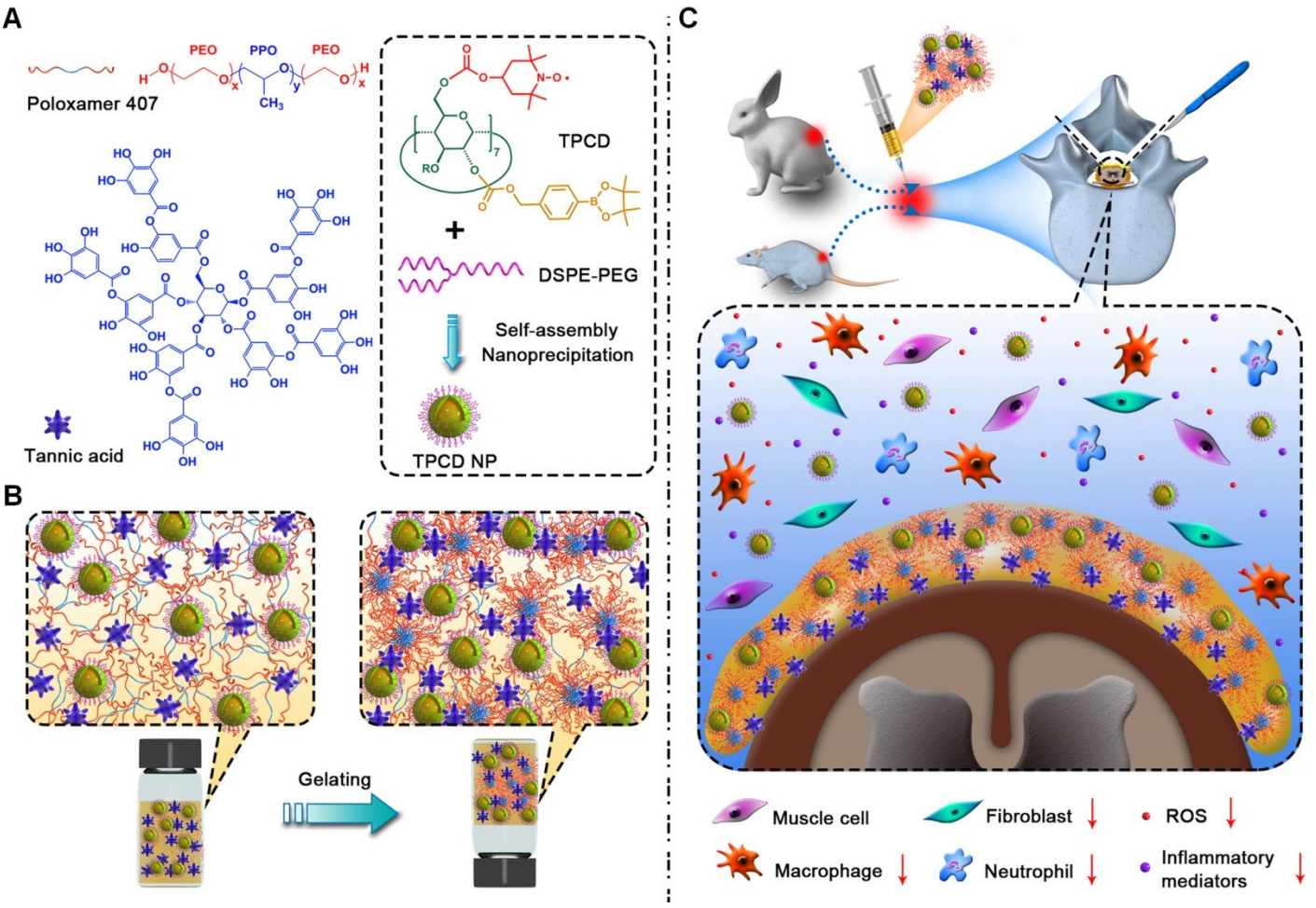

Figure 1. Schematic illustration of engineering of a multifunctional hydrogel for prevention of postoperative epidural fibrosis after lumbar laminectomy. (A) Chemical structures of three functional components for construction of multifunctional hydrogels. (B) Sketch showing temperature-responsive sol-gel transition of the newly designed hydrogel formulation. (C) Prevention of epidural fibrosis and adhesion post laminectomy by local treatment with the engineered advanced hydrogel.

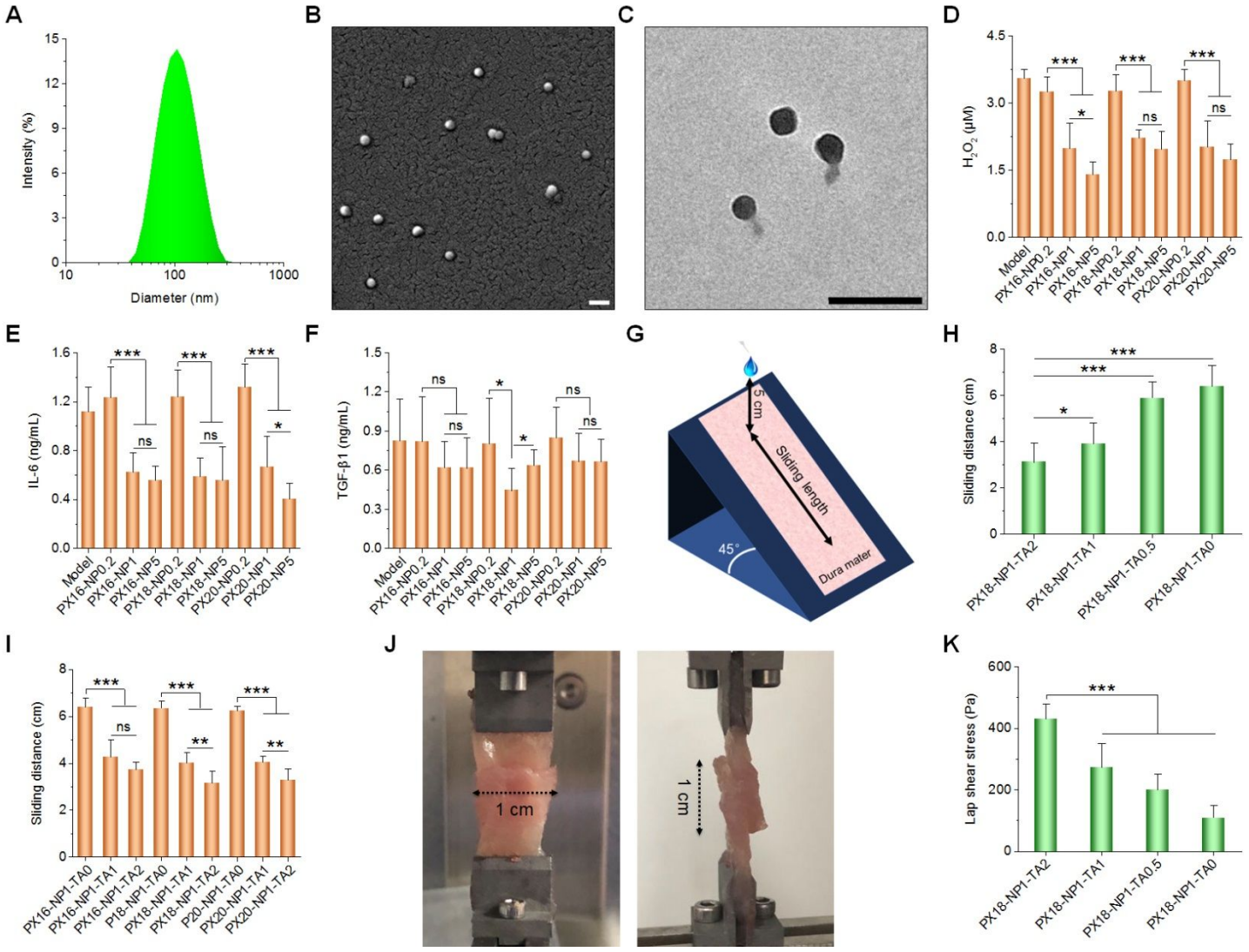

Figure 2. Screening of multifunctional hydrogels for prevention of epidural fibrosis. (A-C) Size distribution (A) as well as SEM (B) and TEM (C) images of TPCD NP. Scale bars, 200 nm. (D-F) Levels of H_2O_2 (D), IL-6 (E), and TGF-β1 (F) in wound lavage from rats subjected to lumbar laminectomy and treatment with different formulations. For different groups, PX concentrations varied from 16, 18, to 20 wt% (defined as PX16, PX18, and PX20, respectively), while TPCD NP changed from 0.2, 1, to 5 mg/mL (defined as NP0.2, NP1, and NP5, respectively). (G) Schematic showing setup of an *in vitro* bioadhesion assessment system based on a tilted plane covered with bovine dura mater. (H) The quantified sliding distance for PX/TPCD NP hydrogels containing different contents of TA. TA0, TA0.5, TA1, and TA2 denote formulations containing 0, 0.5, 1, and 2 wt% TA, respectively. (I) The sliding distance of hydrogels with different contents of PX and TA. (J) Digital photos showing adhesion force test setups. (K) Measured lap shear stress between rat muscle tissues bound together with PX/TPCD NP hydrogels containing different contents of TA. Data are presented as mean ± SD (n ≥ 6). *P < 0.05, **P < 0.005, ***P < 0.0005; ns, no significance.

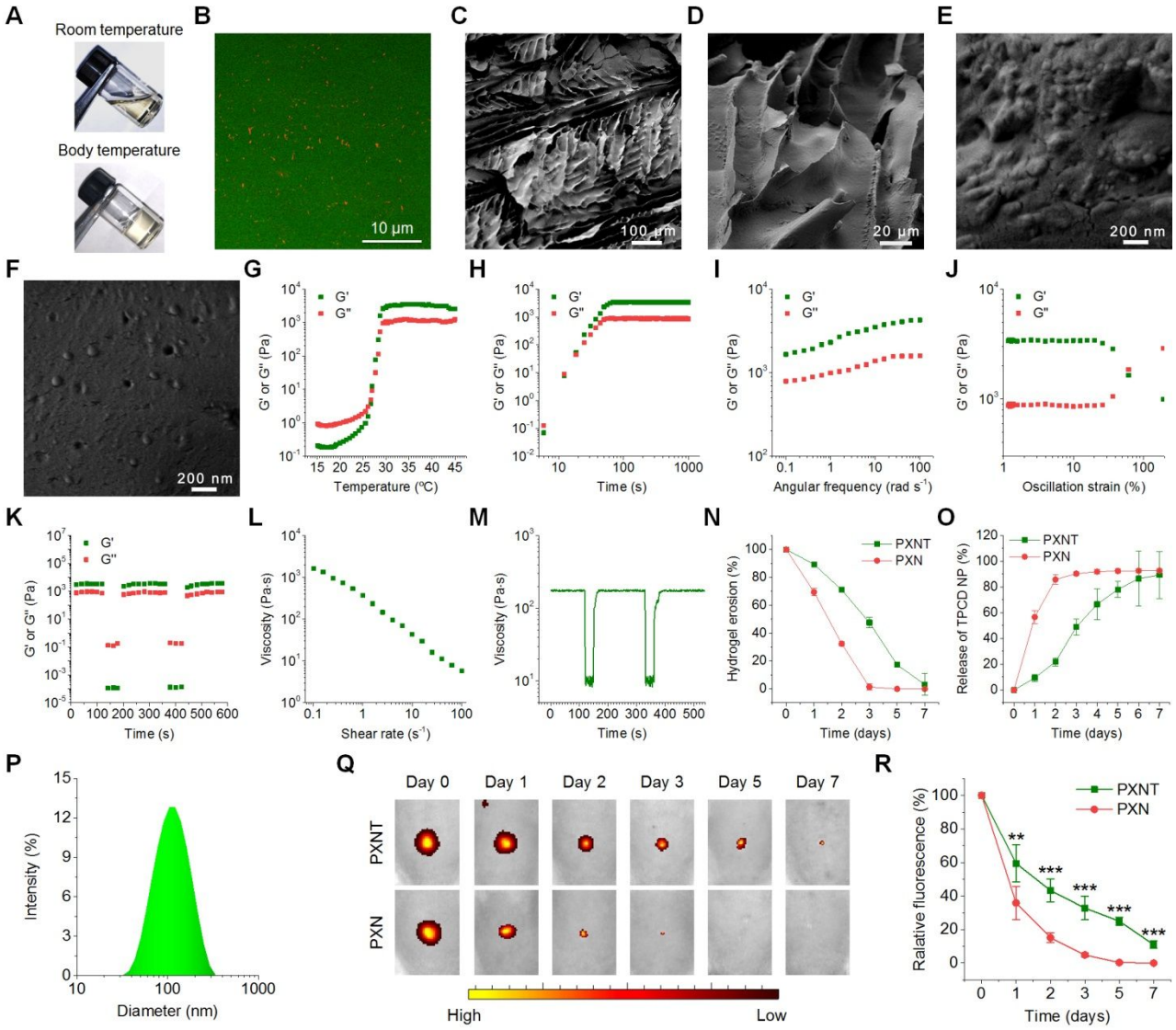

Figure 3. Physicochemical, rheological, and *in vitro/in vivo* erosion properties of PXNT hydrogels. (A) Digitals photos illustrating the sol-gel transition of aqueous solution of PXNT at 37°C. (B) A typical fluorescence image of PXNT hydrogel containing FITC-labeled-PX (green) and Cy5-labeled TPCD NP (red). (C-E) SEM images illustrating fracture surface of PXNT hydrogel at varied resolutions. (F) SEM image showing surface morphology of PXNT hydrogel. (G) Temperature-dependent rheology of PXNT solution ($\omega = 10$ rad s^{-1}, $\varepsilon = 2\%$). (H) Oscillatory time-dependent rheology of PXNT hydrogel at 37°C ($\omega = 10$ rad s^{-1}, $\varepsilon = 2\%$). (I) Frequency-dependent rheology of PXNT hydrogel at 37°C ($\varepsilon = 2\%$). (J) Oscillatory strain-sweep tests of PXNT hydrogel at 37°C ($\omega = 10$ rad s^{-1}). (K) Step-strain measurements of PXNT hydrogel with relatively high (200%) and low (2%) strains to show self-healing performance at 37°C ($\omega = 10$ rad s^{-1}). (L) The shear-thinning behavior of PXNT hydrogel indicated by steady-shear rheology. (M) Step-shear measurements of PXNT hydrogel with high (100 s^{-1}) and low (0.1 s^{-1}) shear rates to demonstrate flow-based self-healing capability. (N) *In vitro* erosion of PXNT or PXN hydrogel in 0.9% saline at 37°C. Data show percentage values of retained hydrogel weight at defined time points. (O) *In vitro* release of TPCD NP from PXNT or PXN hydrogel at 37°C. (P) Size distribution of TPCD NP released from PXNT hydrogel. (Q-R) Real-time *in vivo* images (Q) and quantitative data (R) indicating *in situ* retention of PXNT or PXN hydrogel containing Cy7.5-labeled TPCD NP in rats after intramuscular injection. G′, storage modulus; G″, loss modulus. Data in (N,O,R) are presented as mean ± SD (n = 6). **P < 0.005, ***P < 0.0005.

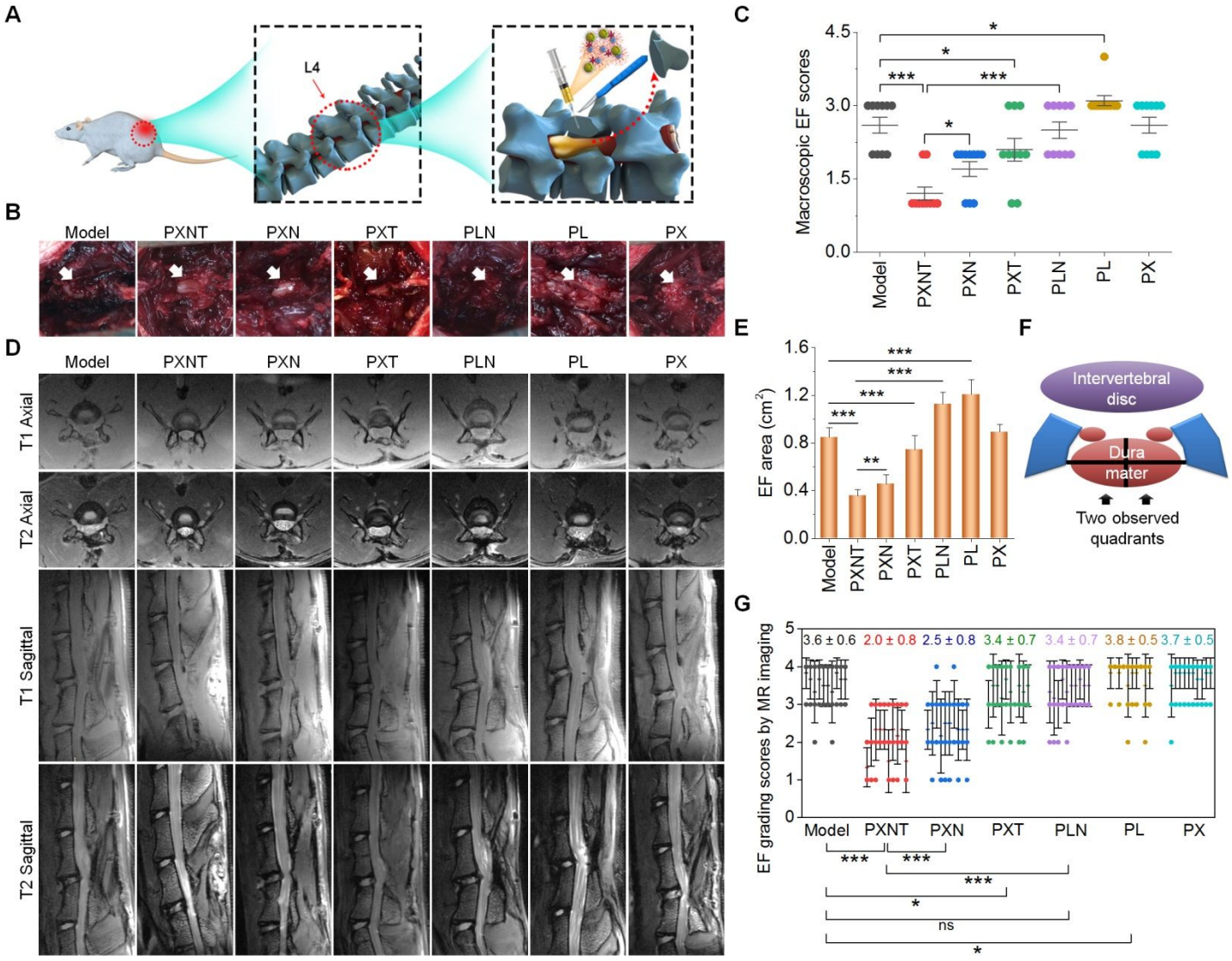

Figure 4. Prevention of epidural fibrosis and adhesion by local treatment with PXNT in rats. (A) Sketch of laminectomy and treatment regimens. (B) Macroscopic observation of laminectomy sites after 8 weeks of treatment. White arrows indicate the location of dura mater. (C) Epidural fibrosis (EF) scores by macroscopic assessment. (D) T1/T2-weighted axial and sagittal MR images of laminectomy sites after 8 weeks of treatment. (E) Quantification of the EF area according to MR images. (F-G) Schematic illustration of axial MR signals used for EF scoring (F) and EF grading scores (G). Data are presented as mean ± SD (n = 10). *P < 0.05, **P < 0.005, ***P < 0.0005; ns, no significance.

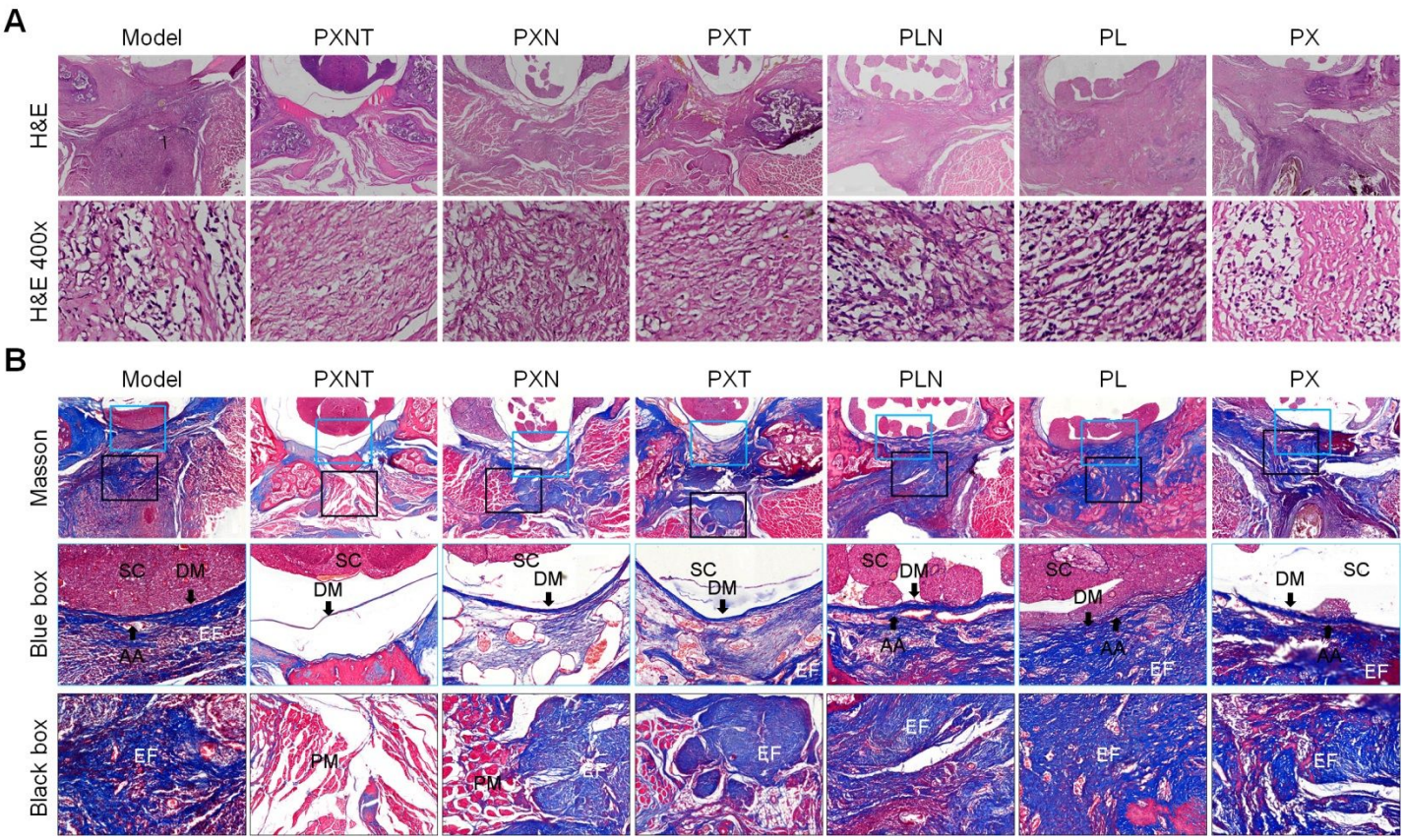

Figure 5. Histological analyses after different treatments. (A) Hematoxylin and eosin (H&E)-stained sections of laminectomy sites at week 8 post-operation. The high-resolution images in the low panel show fibroblast infiltration grades as indicated by H&E-stained epidural fibrosis tissues. (B) Masson-stained sections of laminectomy sites. The regions of interest as indicated by blue and black rectangles are illustrated in the corresponding high-magnification images in the middle and lower panels. AA, adhesion area; DM, dura mater; EF, epidural fibrosis; PM, paravertebral muscle; SC, spinal cord.

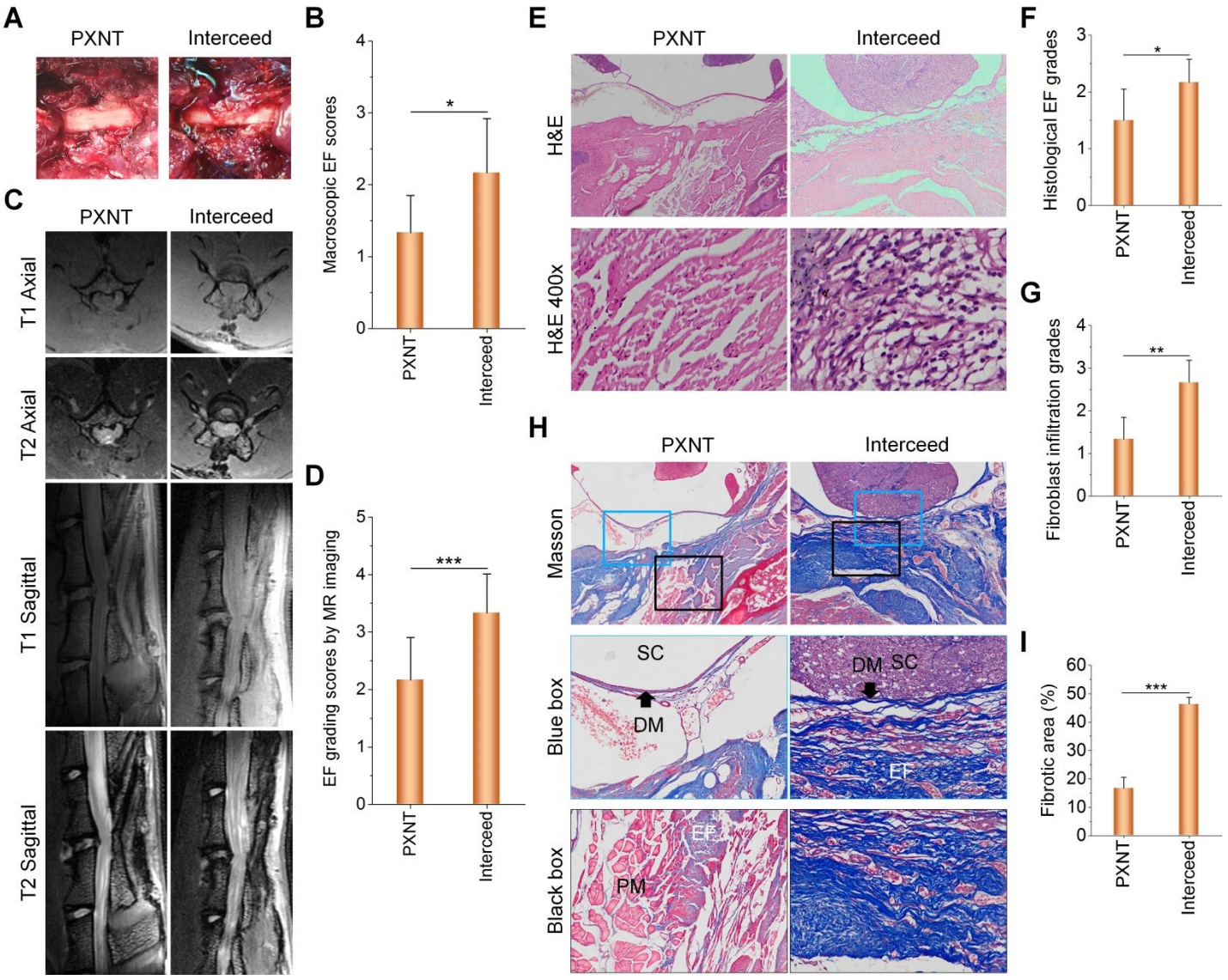

Figure 6. Comparison of anti-fibrosis and anti-adhesion effects of PXNT hydrogel with a commercial adhesion barrier Interceed in rats. (A-B) Macroscopic observation of laminectomy sites (A) and the quantified EF scores (B) after 3 weeks of treatment. (C-D) T1/T2-weighted axial and sagittal MR images of laminectomy sites (C) and quantified EF grading scores (D). (E) H&E-stained sections of laminectomy sites. The high resolution images in the low panel show fibroblast infiltration grades. (F) Quantitative analysis of EF grades. (G) Quantified fibroblast infiltration grades according to H&E-stained sections at high resolution (400×). (H) Masson-stained sections of laminectomy sites. Images in the middle and lower panels show zoomed in regions of interest as indicated by blue and black rectangles in the upper panel. (I) Quantified percentages of fibrotic areas based on Masson-stained sections. Data are presented as mean ± SD (n = 6). *P < 0.05, **P < 0.005, ***P < 0.0005.

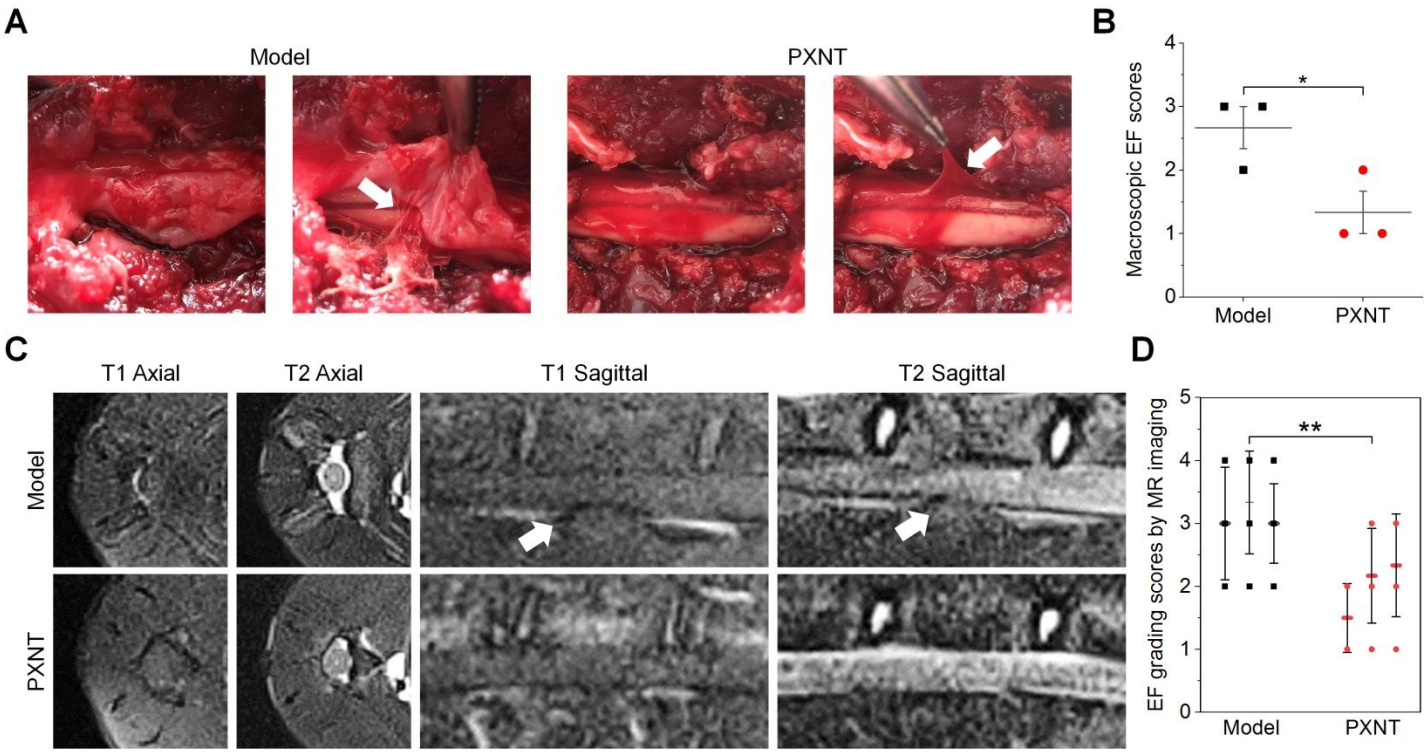

Figure 7. Prevention of epidural fibrosis and adhesion by local treatment with PXNT in rabbits. (A-B) Macroscopic observation of laminectomy sites (A) and quantified EF scores after 3 weeks of treatment (B). White arrows indicate the relationship between the peridural tissue and dura mater. (C-D) T1/T2-weighted axial and sagittal MR images of laminectomy sites (C) and quantified EF grading scores (D). White arrows indicate the peridural fibrosis tissue adhered to the dura mater. Data are presented as mean ± SD (n = 3). *P < 0.05, **P < 0.005.

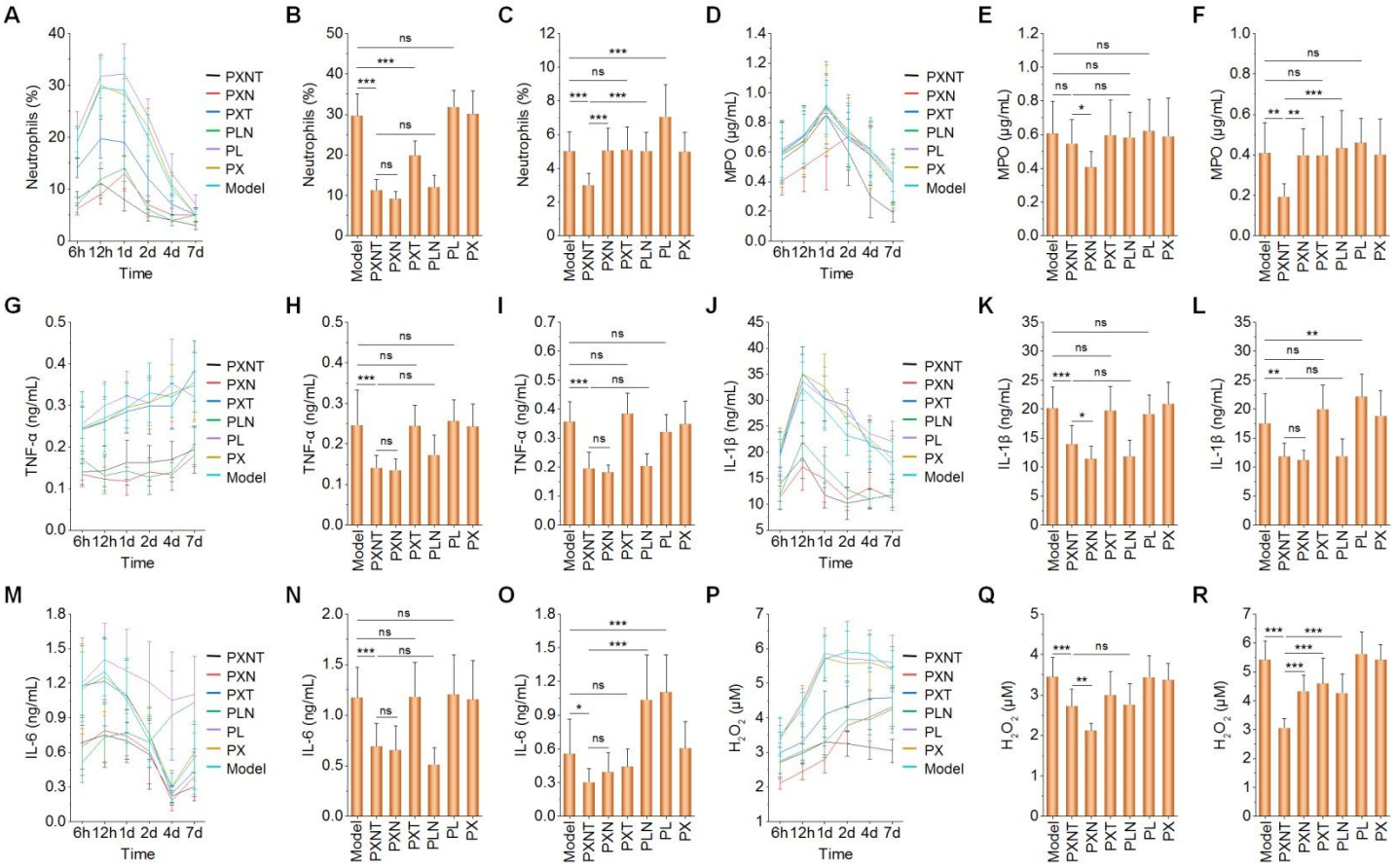

Figure 8. Inflammatory responses at laminectomy sites in rats after different treatments. (A) Changes in neutrophil counts in wound lavage fluid at various time points. (B-C) Quantified neutrophil counts at 12 h (B) and day 7 (C) postlaminectomy. (D) Changing profiles in the levels of MPO in wound lavage during the first 7 days after operation and different treatments. (E-F) Comparison of the MPO levels at 6 h (E) or day 7 (F) between varied groups. (G) Changes in the TNF-α levels in wound lavage fluid. (H-I) Comparison of TNF-α levels at 6 h (H) or day 7 (I) post-operation. (J) IL-1β levels in wound lavage. (K-L) IL-1β levels at 6 h (K) or day 7 (L) post-operation. (M) Changes in IL-6 levels in wound lavage fluid. (N-O) Comparison of IL-6 levels at 6 h (N) or day 7 (O). (P) H_2O_2 levels in wound lavage fluid. (Q-R) Comparisons of H_2O_2 levels at 6 h (Q) or day 7 (R). Data are presented as mean ± SD (n = 12). Statistical significance was assessed by one-way ANOVA tests. *P < 0.05, **P < 0.005, ***P < 0.0005; ns, no significance.

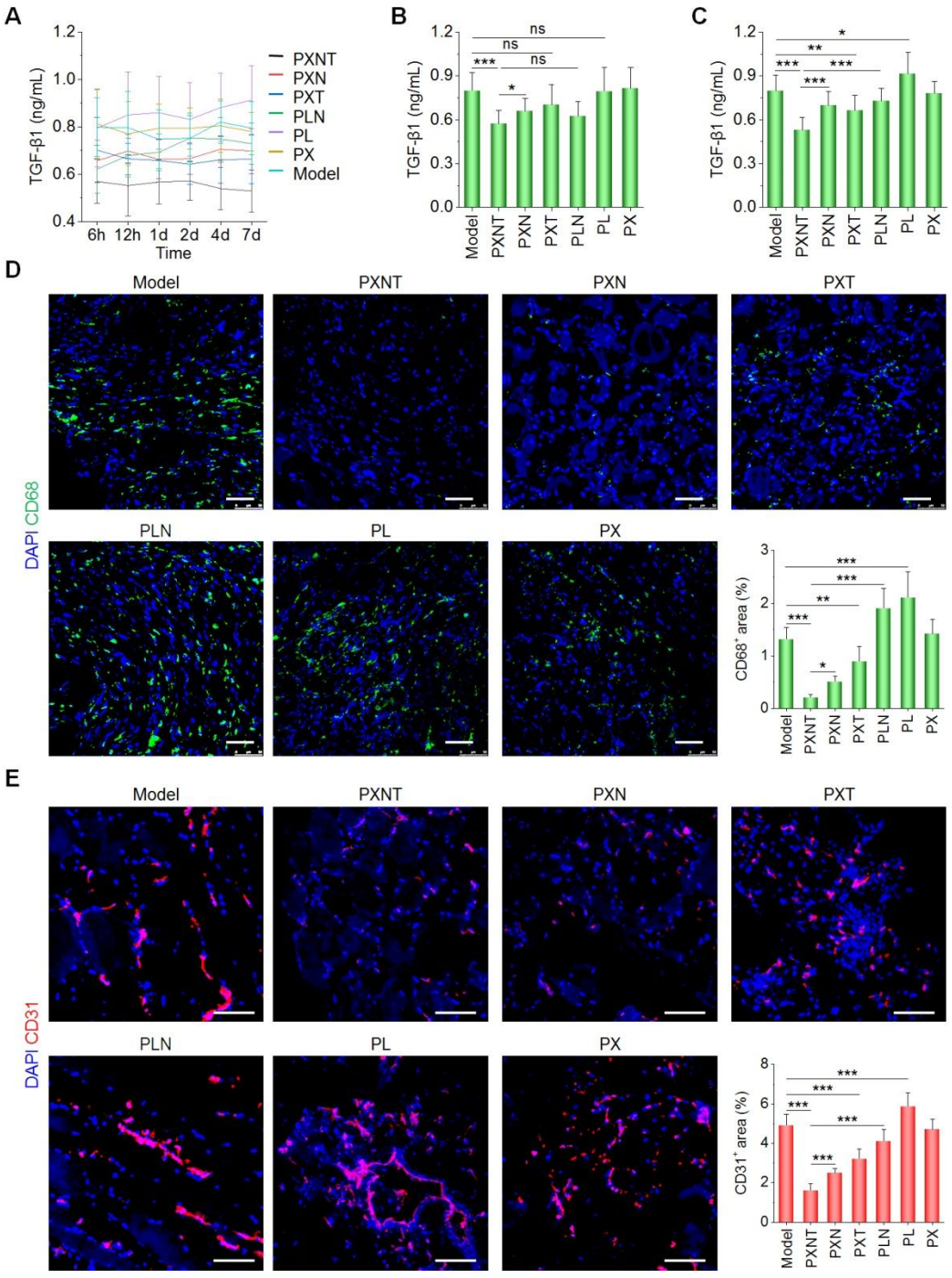

Figure 9. Changes in TGF-β1 levels in wound lavage and immunofluorescence analysis of macrophage count and neovascularization at laminectomy sites during and after treatment with different formulations. (A) TGF-β1 levels in wound lavage fluid at varied time points. (B-C) Comparisons of TGF-β1 levels at 6 h (B) or day 7 (C). (D) Immunofluorescence images indicate $CD68^+$ macrophages (green) and quantitative analysis of $CD68^+$ area. (E) Representative immunofluorescence images showing the presence of new vessels and quantitative analysis of $CD31^+$ area. The endothelial cells were stained with fluorescent CD31 antibody (red), while nuclei were stained with DAPI (blue). Scale bars: 50 μm (D), 100 μm (E). Data are presented as mean ± SD (n = 10). Statistical significance was assessed by one-way ANOVA tests. *P < 0.05, **P < 0.005, ***P < 0.0005; ns, no significance.

Table of Contents Graphic (TOC)